Mathematical Modeling and Simulations of Traffic Flow

by

Jiah Song

A dissertation submitted in partial fulfillment
of the requirements for the degree of
Doctor of Philosophy
(Applied and Interdisciplinary Mathematics)
in The University of Michigan
2019

Doctoral Committee:

Professor Smadar Karni, Co-Chair
Professor Romesh Saigal, Co-Chair
Professor Robert Krasny
Professor Philip Roe

Jiah Song

jiahsong@umich.edu

ORCID iD: 0000-0003-4317-2286

To Leah and Seonghoon with all my love.

ACKNOWLEDGEMENTS

First, I want to express my sincere gratitude to my advisors Professors Smadar Karni and Romesh Saigal. I am especially thankful for Professor Karni's patient guidance, constant support, and kind encouragement. She is a role model of me who can be incredibly patient, brilliant and successful. Professor Saigal is an incredible mentor who provided inspired and valuable advice whenever I seek for a help. I especially thank for his help in finding a job. I was very lucky to have them as my advisors who are immensely approachable. We had so many productive conversation about the research.

I would like to thank my committee members Professors Philip Roe and Robert Krasny for taking their time to allow me to present my research, and offering useful comments to this dissertation.

I also thank all the friends that I have made here in Michigan, and all the support from the Math department. Thanks to my family and friends in South Korea who always believe in me and support me with your unconditional love.

Lastly, Leah and Seonghoon. Leah, you gave me a new life. Thank you for making me a good person, my forever sunshine. All the work in this dissertation went along with you for the past three years. Seonghoon, this dissertation would have not been able to be complete without your support. I look forward to spending our time after graduation. You are my only hero.

TABLE OF CONTENTS

LIST OF FIGURES

Figure

ABSTRACT

This dissertation concerns modeling and computation of macroscopic fluid-like traffic flow on a single lane road as well as on multilane, coupled with lane changes. We start with single lane models and consider the scalar model, expressing car mass conservation, proposed in the 1950s (Lighthill-Whitham 1955, Richards 1956). This requires a velocity-density closure relation, called Fundamental Diagram. We propose a more realistic closure relation, based on field data fitting. Using a relationship between car headway and flow density, we develop and extend to a new 2x2 system that includes an intra-lane acceleration equation reflecting microscopic flow characteristics. The models are then generalized to multilane traffic flow and incorporate mass exchange terms, as well as inter-lane acceleration terms. We present two types of multilane models that are nonlinear hyperbolic equations: (i) scalar models and (ii) 2x2 systems. Both types are formulated by establishing lane changing conditions from drivers' perspectives and incorporating them into source terms. Consideration for lane changing includes the potential for velocity gain and available space. Using Roe-type upwind scheme, we reproduce realistic flow patterns such as stop-and-go flow and study the influence of lane changing and lane reduction on flow capacity.

CHAPTER I

Introduction

The scope of this dissertation encompasses mathematical models, numerical computations of traffic flow, and understanding its essential fundamentals based on field data. Chapter I presents the mathematical structure and its numerical aspects in section 1.1 and the description of data being utilized in section 1.2.

Two classes of models are taken into account in describing traffic flow: microscopic and macroscopic descriptions. The former is based on individual vehicles' motion, and the latter is concerned with average behavior. Our interest is mainly in macroscopic understanding that naturally leads to the hyperbolic partial differential equations (PDEs). The following, therefore, sheds light on theory and numerical methods of nonlinear hyperbolic equations.

1.1 Hyperbolic Conservation Laws

1.1.1 Mathematical Theory

We start by stating a system of hyperbolic conservation laws with an initial condition

$$\begin{cases} \partial_t W + \partial_x F(W) &= 0 \\ W(x,0) &= W_0(x) \end{cases} \tag{1.1}$$

where t is the time, x is the space, $W = W(x,t)$ is a vector of n conserved variables, and $F(W)$ is a vector of n fluxes. For brevity, x and t are omitted. Here

$$\begin{aligned} W &= (w_1, w_2, \cdots, w_n)^T, \\ &\text{and} \\ F(W) &= (f_1(W), f_2(W), \cdots, f_n(W))^T. \end{aligned}$$

We deal with one-dimensional case in x but note that this may be extended to multi-dimensions as needed. Many practical problems, including gas dynamics, a spiral galaxy, shallow water waves, traffic flow etc, involve conserved quantities. Therefore, the field of hyperbolic conservation laws provides the theoretical underpinnings for modeling them.

In a quasilinear form, (1.1) can be put into the following frame:

$$\begin{cases} \partial_t W + A(W)\partial_x W = 0 \\ W(x,0) = W_0(x) \end{cases} \tag{1.2}$$

where

$$A(W) = F'(W) = \frac{\partial F(W)}{\partial W} = \begin{pmatrix} A_{11} & \cdots & A_{1n} \\ \cdots & A_{ij} = \frac{\partial f_i}{\partial w_j} & \cdots \\ A_{n1} & \cdots & A_{nn} \end{pmatrix}$$

is the Jacobian matrix of $F(W)$. (1.1) is linear if $A(W)$ returns a constant matrix, or nonlinear otherwise. (1.1) is hyperbolic if $A(W)$ has n real eigenvalues and linearly independent n eigenvectors. Derivation of hyperbolic systems can be found in many books [32, 35, 51, 53]. We will later focus on the derivation of scalar equation in terms of traffic flow in section 3.1.1.

Hyperbolic PDE features characteristic curves along which information propagates

at a finite speed. Let us take the Burgers' equation for illustrating characteristics

$$\text{(1.3)} \qquad \begin{cases} \partial_t w + \partial_x f(w) &= 0 \\ w(x,0) &= w_0(x) \end{cases}$$

where $f(w) = \frac{w^2}{2}$. Characteristic curve, $x(t)$, is chosen so that

$$\begin{aligned} \tfrac{d}{dt} w(x(t),t) &= \partial_t w + \tfrac{dx}{dt}\partial_x w \\ &= 0. \end{aligned}$$

Note that w is constant along the curve satisfying $x'(t) = f'(w) = w$, and the curve is a straight line. For smooth initial condition, we can construct a solution implicitly with characteristics:

$$w(x,t) = w_0(x - f'(w)t) = w_0(x - wt).$$

This seems like we completely solved a Burgers' equation, but indeed it is only valid up until the solution is smooth. When faster information along its characteristics overtakes slower one, the characteristics intersect. So what will happen is the smoothness breaks, and the PDE becomes invalid because of a multi-valued solution. Allowing discontinuity, so-called shock wave, is a way to extend the solution beyond the time when the solution becomes multi-valued. The jump condition across the discontinuity relies on an integral form of the conservation laws.

The integral form of (1.1) on domain $[x_1,\ x_2]$ and time interval $[t_1,\ t_2]$ reads

$$\text{(1.4)} \qquad \int_{x_1}^{x_2} W(x,t_2)\ dx = \int_{x_1}^{x_2} W(x,t_1)\ dx + \int_{t_1}^{t_2} \Big(F(W(x_1,t)) - F(W(x_2,t))\Big)\ dt.$$

This provides an insight of shock jump condition. As Figure 1.1 indicates, in an infinitesimal area including a shock path, (1.4) can be approximated by

$$W_L \Delta x \approx W_R \Delta x + \Delta t (F_L - F_R)$$

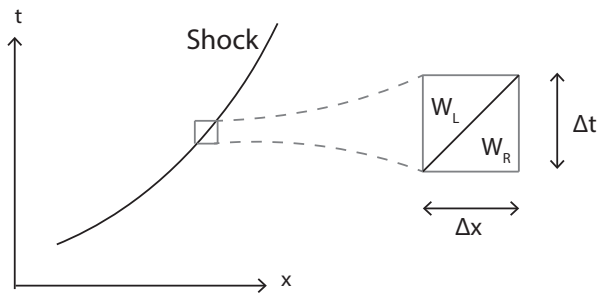

Figure 1.1: Shock jump condition

which leads to the Rankine-Hugoniot jump condition

$$[F] = F_R - F_L = \frac{\Delta x}{\Delta t}(W_R - W_L) = s[W]$$

where $[\cdot] = (\cdot)_R - (\cdot)_L$ and shock speed $s \approx \frac{\Delta x}{\Delta t}$. This shows that the shock jump condition ensures the conservation laws.

The solution that is piecewise smooth separated by discontinuity curves and satisfies PDE in smooth parts and shock jump condition across discontinuities is called a weak solution. Weak solutions satisfy

$$\int_{-\infty}^{+\infty} W\phi_t \, dx + \int_0^{\infty} F(W)\phi_x \, dt = \int_{-\infty}^{+\infty} W(x,0)\phi(x,0) \, dx \tag{1.5}$$

for all test functions ϕ that are smooth and of compact support. See [51, 35] for details. Note that smoothness in W is not necessary anymore by transferring its requirement to test functions ϕ. It turns out that weak solutions are not unique. The physically relevant solution can be obtained by the principle of stability or checking the Entropy condition. One can either regularize the initial data by a small amount or the equation itself by adding a small viscous term, and then apply limiting process to find the vanishing viscosity solution. This is based on the principle that solution should be stable to small perturbations: if problem is changed by a small amount, then the solution should change by a small amount. The Entropy condition is the condition that picks a solution of physical relevance among many weak solutions. A

discontinuity propagating with speed s satisfies the Lax Entropy condition if

$$f'(w_L) > s > f'(w_R)$$

for convex f [32]. Geometrically it says that shock wave is admissible if characteristics converge into the shock. A more general entropy condition due to Oleinik, valid for non-convex f, says about the entropy solution with speed s: all discontinuities have the property that

$$\frac{f(w) - f(w_L)}{w - w_L} \geq s \geq \frac{f(w) - f(w_R)}{w - w_R}$$

for all w between w_L and w_R [51]. Another approach to formulate the Entropy condition is to use entropy functions and entropy fluxes. See [35] for details.

The Riemann Problem associated with a hyperbolic conservation laws is to find a solution, called the Riemann solution, with an initial condition:

$$W(x,0) = \begin{cases} W_L, & x < 0 \\ W_R, & x > 0. \end{cases} \tag{1.6}$$

Understanding the Riemann solution provides both insights into the physical system itself and critical numerical perspectives due to the emergence of shock phenomenon.

Example I.1. *Consider Burgers' equation* (1.3) *with*

$$w(x,0) = \begin{cases} w_L = 1, & x < 0 \\ w_R = 0, & x > 0. \end{cases}$$

Characteristics are straight lines starting from the initial profile, see Figure 1.2a. They are converging as fast information with speed $f'(1)$ catches up with the slow information with speed $f'(0)$. Therefore, the Riemann solution is a shock wave connecting two states w_L and w_R, traveling with speed

$$s = \frac{[f]}{[w]} = \frac{\frac{1}{2}w_R^2 - \frac{1}{2}w_L^2}{w_R - w_L} = \frac{1}{2},$$

see Figure 1.2b. □

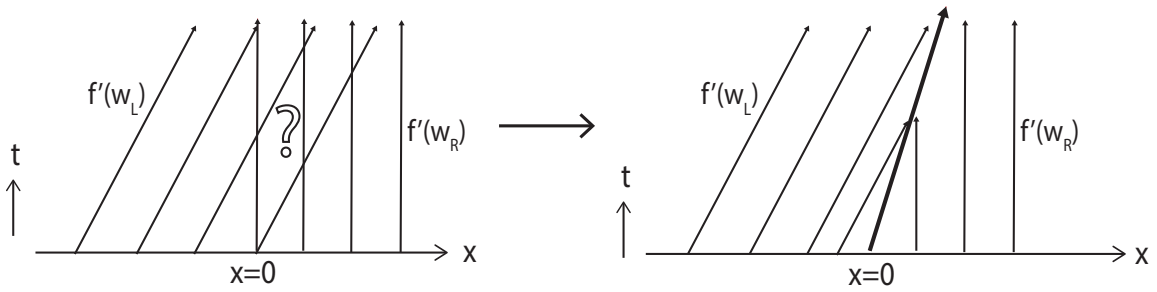

(a) Characteristics creating a shock wave

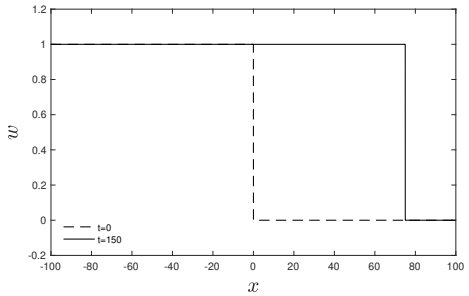

(b) Riemann solution

Figure 1.2: Example I.1

Example I.2. *Now consider (1.3) with*

$$w(x,0) = \begin{cases} w_L = 0, & x < 0 \\ w_R = 1, & x > 0. \end{cases}$$

Characteristics are nondecreasing as x increases, see Figure 1.3a. One may consider a weak solution that contains a discontinuity with speed $\frac{f(w_L)-f(w_R)}{w_L-w_R}$. However, this solution violates the Entropy condition. Therefore, the Riemann solution is a rarefaction wave as in Figure 1.3b □

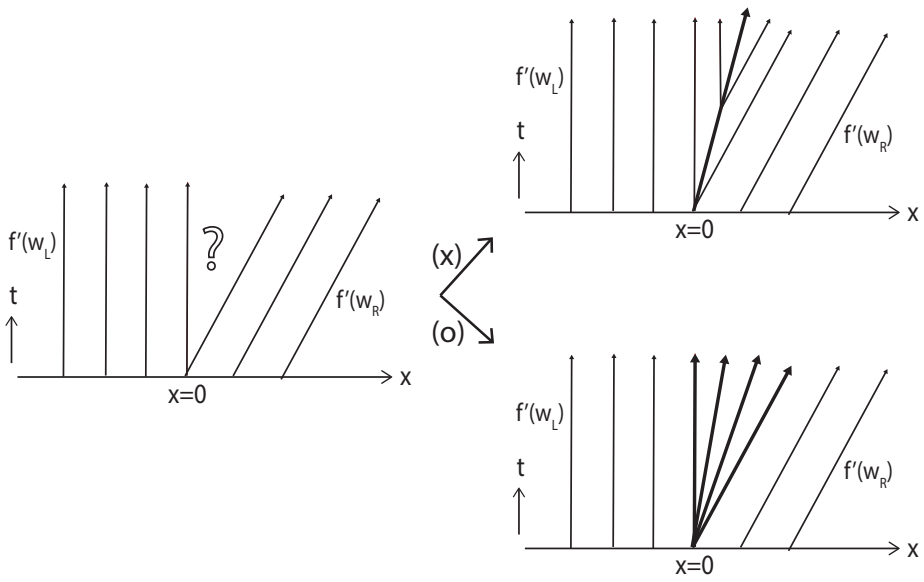

(a) Characteristics creating a rarefaction wave

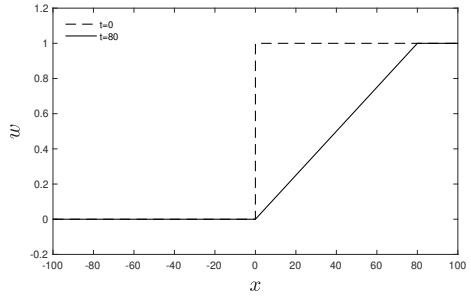

(b) Riemann solution

Figure 1.3: Example I.2

1.1.2 Numerical Methods

Foundational numerical methods in particular finite volume method (FVM) is focused here and will be used throughout this dissertation for PDE-based computations. Let us consider

$$\partial_t W + \partial_x F(W) = 0. \tag{1.7}$$

FVM deals with a cell average by defining it at time t_n over $[x_{j-\frac{1}{2}}, x_{j+\frac{1}{2}}]$ as

$$W_j^n \approx \frac{1}{\Delta x} \int_{x_{j-\frac{1}{2}}}^{x_{j+\frac{1}{2}}} W(x, t_n)\, dx.$$

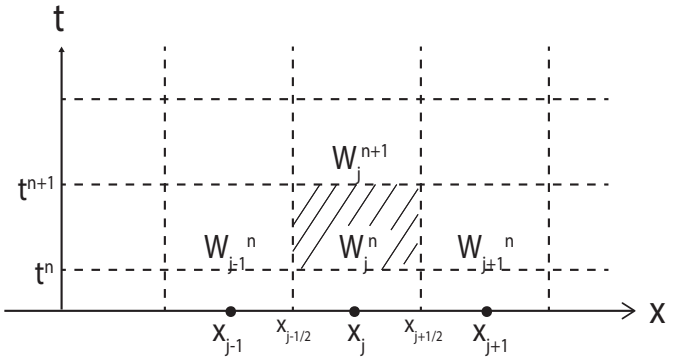

Figure 1.4: Schematic for numerical computation

Here Δx is a mesh width and Δt is a time step. FVM approximates the integral form (1.4) of (1.7) on the shaded region in Figure 1.4. One numerical feature in conservation laws is to maintain its conservation. A conservative method requires

$$W_j^{n+1} = W_j^n - \frac{\Delta t}{\Delta x}[F_{j+\frac{1}{2}} - F_{j-\frac{1}{2}}] \tag{1.8}$$

where $F_{j+\frac{1}{2}}$ is a numerical flux defined at the cell interface as some function of, for example, W_j^n and W_{j+1}^n. Different choices of numerical flux provide different methods. There is a necessary stability condition, called CFL condition, that the domain of dependence of numerical method should contain the domain of dependence of the PDE. This condition was originally derived for finite difference methods for PDEs by Courant, Friedrichs, and Lewy [13]. Nonlinear hyperbolic systems yields:

$$\left|\lambda_p(W_j^n)\frac{\Delta t}{\Delta x}\right| \leq 1 \tag{1.9}$$

for all p at each W_j^n, where λ_p is the p th eigenvalue of the Jacobian matrix $F'(W)$. Lax-Wedroff theorem says that if numerical solutions by a conservative method converge to some function as the grid is refined, then this function is a weak solution of the conservation law [31]. Godunov's scheme is one conservative method proposed in 1959 [18]. It numerically solves exact Riemann solution on every cell interface, which is expensive. We introduce the Upwind scheme by linearizing the Jacobian matrix

at each cell interface developed by Roe [48, 49, 50]. This is one kind of approximate Riemann solvers. In a quasilinear form, (1.7) becomes

$$\partial_t W + A(W)\partial_x W = 0. \tag{1.10}$$

Roe's method approximates $A(W)$ at $x_{j+\frac{1}{2}}$ by $\bar{A}(W_j, W_{j+1})$ satisfying

1. $\bar{A}(W_j, W_{j+1})(W_j - W_{j+1}) = F(W_j) - F(W_{j+1})$,
2. $\bar{A}(W_j, W_{j+1})$ is diagonalizable with real eigenvalues, and
3. $\bar{A}(W_j, W_{j+1}) \to F'(\bar{W})$ smoothly as $W_j, W_{j+1} \to \bar{W}$.

Unless we deal with a scalar model, the choice of $\bar{A}$ is not unique. The scheme can be expressed by

$$W_j^{n+1} = W_j^n - \frac{\Delta t}{\Delta x}\Big\{\bar{A}^+_{j-\frac{1}{2}}(W_j^n - W_{j-1}^n) + \bar{A}^-_{j+\frac{1}{2}}(W_{j+1}^n - W_j^n)\Big\} \tag{1.11}$$

and

$$\bar{A}^+\Delta W = \sum_{\bar{\lambda}_k>0} \alpha_k \bar{\lambda}_k \bar{r}_k,\ \ \bar{A}^-\Delta W = \sum_{\bar{\lambda}_k<0} \alpha_k \bar{\lambda}_k \bar{r}_k \tag{1.12}$$

where $\Delta(\cdot) = (\cdot)_{i+1} - (\cdot)_i$. Here $\bar{r}_k/\bar{\lambda}_k$ are the eigenvectors/eigenvalues of local linearization $\bar{A}$ at $x_{j+\frac{1}{2}}$. Because of the second requirement, wave strengths α_k can be uniquely determined:

$$\Delta W = \sum_k \alpha_k \bar{r}_k.$$

The first requirement implies that this method guarantees conservation.

When there is a source term, the hyperbolic balance laws in a quasilinear form read

$$\partial_t W + A(W)\partial_x W = S(W). \tag{1.13}$$

Source term, $S(W)$, can be treated by means of Upwind as well. The scheme includes the source term by being projected onto the eigenstructure of $\bar{A}$ [50]:

$$W_j^{n+1} = W_j^n - \frac{\Delta t}{\Delta x}\Big\{\big(\bar{A}^+_{j-\frac{1}{2}}\Delta W^n - \Delta x \bar{S}^+_{j-\frac{1}{2}}\big) + \big(\bar{A}^-_{j+\frac{1}{2}}\Delta W^n - \Delta x \bar{S}^-_{j+\frac{1}{2}}\big)\Big\} \tag{1.14}$$

where

(1.15)

$$\bar{A}^+\Delta W - \Delta x \bar{S}^+ = \sum_{\bar{\lambda}_k>0}(\alpha_k\bar{\lambda}_k - \Delta x\beta_k)\bar{r}_k,\ \bar{A}^-\Delta W - \Delta x \bar{S}^- = \sum_{\bar{\lambda}_k<0}(\alpha_k\bar{\lambda}_k - \Delta x\beta_k)\bar{r}_k.$$

Wave strengths α_k and β_k can be determined:

$$\Delta W = \sum_k \alpha_k \bar{r}_k,\ \bar{S} = \sum_k \beta_k \bar{r}_k$$

where $\bar{S}$ is some averaging source term at the cell interface.

Closing Remarks: More details on theory and different numerical methods including higher order schemes can be found in [32, 51, 53, 35].

1.2 Traffic Field Data

This section describes traffic field data used in this dissertation. Dataset was collected under Next Generation SIMulation (NGSIM) project[1]. Data from the innermost lane of US Highway 101 (US 101) and lane 2[2] of Interstate 80 (I-80) were used because it is less likely to have trucks or large vehicles that may have different driving maneuver than regular cars, and less vehicles changing lanes. US 101 data records vehicle trajectories and instantaneous velocity on the southbound of US 101 in Los Angeles, CA, between 7:50 a.m. and 8:35 a.m. on June 15, 2005. The study area is approximately $2,100$ feet in length. Vehicle trajectories of I-80 data are recorded on northbound direction of Interstate 80 in San Francisco, CA, between 5:00

[1] NGSIM dataset is open to public for the purpose of research: https://data.transportation.gov.
[2] Lane 1 of I-80 is designated as high-occupancy vehicle lane.

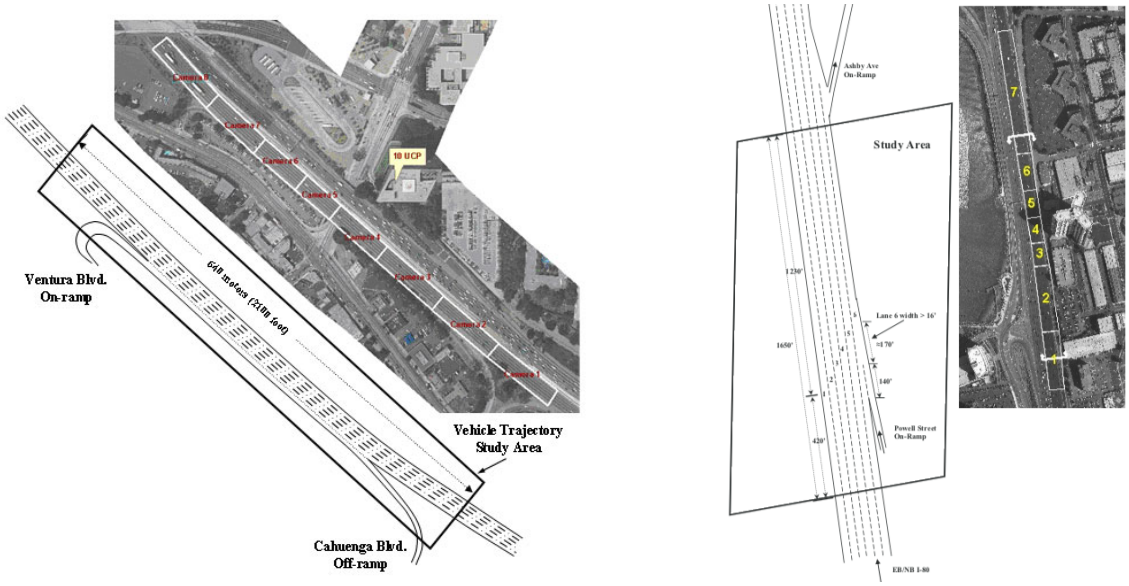

(a) US 101 (b) I-80

Figure 1.5: Study area schematic and camera coverage

p.m. and 5:30 p.m. on April 13, 2005. The site is approximately 1,650 feet in length. More specific study area location is in Figure 1.5. Both US 101 and I-80 data provide the precise location of every vehicle within the study area every one-tenth of a second along with detailed lane positions. See Figure 1.6a for the first 3 minutes of vehicle trajectories. Our objective is to extract a manageable macroscopic information from this microscopic-collected dataset without losing much information. Therefore

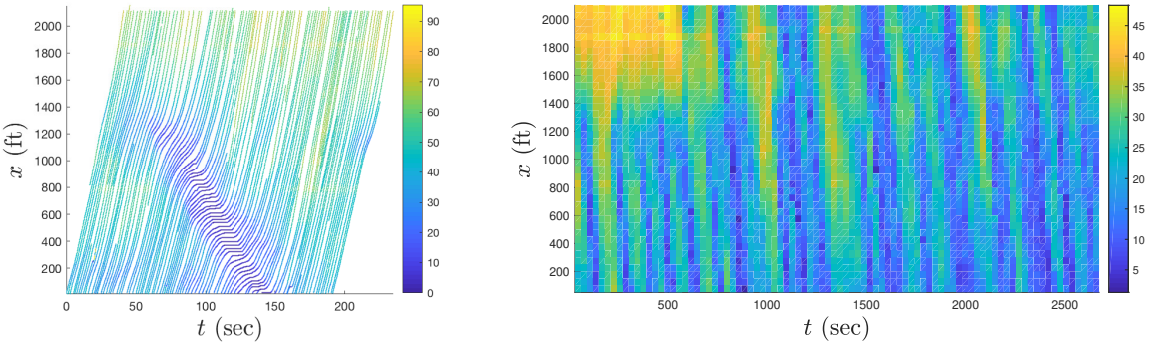

(a) Vehicle trajectories color-coded with instantaneous velocity (ft/sec) from 7:50 am - 7:53 am

(b) Mean velocity map (mph) from 7:50 am - 8:35 am

Figure 1.6: Two velocity visual representations of US 101 (lane 1)

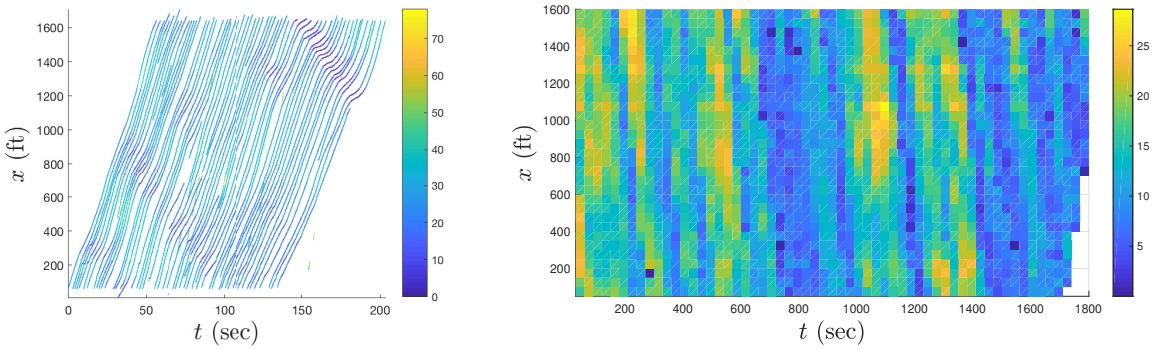

(a) Vehicle trajectories color-coded with instantaneous velocity (ft/sec) from 5:00 pm - 5:02 pm

(b) Mean velocity map (mph) from 5:00 pm - 5:30 pm

Figure 1.7: Two velocity visual representations of I-80 (lane 2)

the overall emphasis in this section is on the method how we transform given microscopic format into macroscopic format. The variables describing macroscopic flow are: density $\rho(x,t)$= number of vehicles per unit length, average velocity $v(x,t)$, and flux or the rate of flow $f(x,t)$= number of vehicles per unit time. Moreover, they are related in a fundamental way that $f(x,t) = \rho(x,t)v(x,t)$. This implies that two variables are enough to describe traffic flow. Hereafter, we drop (x,t) for easy reading. Later we dive into the continuity equation for vehicle conservation that relates these variables. To compute macroscopic variables ρ and v given the trajectory dataset, the $t-x$ plane is discretized by choosing rectangles of $\Delta x = 50$ (feet) and $\Delta t = 30$ (sec)[3] unless we specify otherwise, and the discrete mesh points (x_i, t_j) by $x_i = i\Delta x$ and $t_j = j\Delta t$ are defined. Within each rectangle $[x_i, x_i + \Delta x) \times [t_j, t_j + \Delta t)$, we average the measurement of the speeds of individual vehicles using the space mean speed. Space mean speed is defined as the harmonic mean of speeds traversing a point $x_i + \frac{\Delta x}{2}$ during time Δt: $v = \frac{n}{\sum_{i=1}^{n} 1/v_i}$. f is computed by counting the number

[3] Δx and Δt need to be carefully chosen. If this is too small, information is not aggregated enough and if this is too large, important information may be overlooked.

of vehicles, denoted by N, that pass a point $x_i + \frac{\Delta x}{2}$ during time Δt:

$$\int_{t_j}^{t_j+\Delta t} f \; dt = N \tag{1.16}$$

at $x = x_i + \frac{\Delta x}{2}$ for all $i,\ j$. Then ρ by the fundamental relation $\rho = \frac{f}{v}$. These values are assigned to each rectangle, see Figure 1.6b for an example of average velocity v over entire space and time for US101. We found that the on-ramp is controlled by a ramp meter[4], and this probably accounts for the quasi-periodic pattern in Fig 1.6. The mathematical models of traffic flow that are studied in this dissertation generally neglect lane changing, so we only studied the data from lane 1, which has only one neighboring lane to change into. In fact , it can be deduced from the data in [8] that fewer than half of the vehicles observed did change lanes during the observation, so the data are quite suitable for our analysis. Corresponding data for I-80 is in Figure 1.7. All testing that follows in section 3.1.2 is done on these aggregated ρ and v.

Closing Remarks:

1. Theory, computation, and applications of traffic flow are increasingly recognized as autonomous and connected vehicles have been a rising issue. Full understanding of mixed flow of human and autonomous vehicles requires good knowledge of human-driving models, which are main theme in this work, and from which transportation engineers can benefit.

2. The rest of the dissertation is organized as follows. Chapter II reviews microscopic models and presents its interesting simulation. Chapter III concerns macroscopic models comprehensively: it opens up from existing macroscopic models, and closes by proposing new multilane models. Chapter IV lists the proposed model-based numerical results along with numerical methods. Finally Chapter V concludes

[4]This can be deduced from Google Earth.

the dissertation by summarizing the contribution of this work. Future research topics and potential applications are also highlighted in Chapter V.

CHAPTER II

Microscopic Car-Following Model

As mentioned in Chapter I, mathematically traffic flow can be described by systems of ordinary differential equations (ODEs), known as microscopic car-following models, or PDEs that are macroscopic fluid-like models. The particle-based model illustrates the motion of individual vehicles by taking its acceleration into account. Although the main interest in this dissertation pertains to macroscopic PDE models, we start with understanding how individual vehicles act and communicate each other. This will be used to relate particle-level description to fluid-level description. For this purpose, we review some microscopic models and present some numerical results.

2.1 Literature Review

Car-following model, sometimes referred to as the follow-the-leader model, has been extensively developed since 1950s. Its underlying idea is that (n)th vehicle's response is based on its sensitivity and stimulus from $(n+1)$th vehicle that is assumed to be placed ahead, see Figure 2.1.

$$\text{Response}_n(t) = \text{Sensitivity}_n(t - \tau_n) \cdot \text{Stimulus}_n(t - \tau_n) \tag{2.1}$$

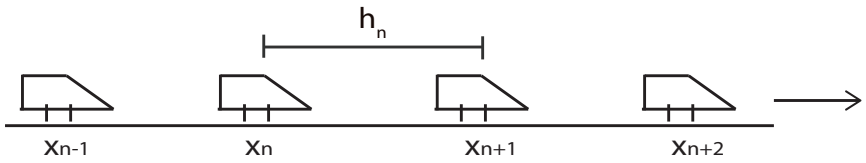

Figure 2.1: Car-following schemetics

where τ_n is reaction time of (n)th driver. Given assumptions that vehicles are identical and drivers react in the same way, same sensitivity for instance, movement of vehicles may be governed by fundamental relation of (2.1). In 1958, Chandler *et al.* studied

$$\ddot{x}_n(t) = \alpha[\dot{x}_{n+1}(t-\tau_n) - \dot{x}_n(t-\tau_n)] \tag{2.2}$$

where $x_n(t)$ is the position of (n)th car at time t, and α is a constant in unit of time^{-1} [10]. $\dot{}$ indicates a derivative taken with respect to t. Response$_n$ in (2.1) is replaced with (n)th drivers' acceleration, Sensitivity$_n$ with a constant parameter, and Stimulus$_n$ with relative speed between $(n+1)$th and (n)th vehicles. This simply illustrates that (n)th vehicle accelerates (or decelerates) when it travels slower (or faster) than $(n+1)$th vehicle. Parameter α in the model is measured by field traffic data. This model is simple but has a drawback that it has a constant sensitivity that is too limited. Since this model, there have been many improvements. In 1959, Gazis *et al.* proposed

$$\ddot{x}_n(t) = \frac{\alpha}{h_n(t-\tau_n)}(\dot{x}_{n+1}(t-\tau_n) - \dot{x}_n(t-\tau_n)) \tag{2.3}$$

where $h_n(t)$=$x_{n+1}(t) - x_n(t)$ is the headway at time t, see again Figure 2.1, and α is a constant [16]. This incorporates headway into sensitivity: $(n)$the vehicle is less affected by the car ahead when headway is large enough, and vice versa. General Motors Nonlinear Model was followed by Gazis *et al.* in 1961:

$$\ddot{x}_n(t) = \alpha\frac{\dot{x}_n(t)^\beta}{h_n(t-\tau_n)^\gamma}(\dot{x}_{n+1}(t-\tau_n) - \dot{x}_n(t-\tau_n)) \tag{2.4}$$

where $\alpha,\ \beta,\ \gamma$ are constants to be determined [17]. Note that (2.2) and (2.3) are special forms of (2.4). More realistic ideas were followed. In 1968, Bexelius developed

$$\ddot{x}_n(t) = \sum_{i=1}^{N} \alpha_i(\dot{x}_{n+i}(t-\tau_n) - \dot{x}_n(t-\tau_n)). \tag{2.5}$$

Here (n)th car's response is not just due to $(n+1)$th car, but also to $(n+i)$th cars for $i = 2, 3, ..., N$ weighed by α_i [7]. In 1993, Ozaki suggested to treat acceleration and deceleration differently, and empirically estimated parameters using (2.4) [45]. Recent work proposed by Zhang in 2002 is

$$\ddot{x}_n(t) = \frac{\dot{x}_{n+1}(t) - \dot{x}_n(t)}{\tau(h_n(t))} \tag{2.6}$$

where τ is the response time [59]. Rather than having a constant factor in sensitivity and reaction time, Zhang uses an idea of response time, denoted by τ, varying with headway. (2.6) was used to derive macroscopic acceleration equation or the continuum version:

$$\partial_t v + v\partial_x v \approx \frac{h}{\tau(h)}\partial_x v \tag{2.7}$$

where v represents the mean velocity and h is the macroscopic headway. Zhang formulated

$$\frac{h}{\tau(h)}\partial_x v = -\rho V'(\rho)\partial_x v$$

where V is some equilibrium velocity that depends on the local density. $\rho V'(\rho)$ can be interpreted as the traffic sound speed at which small traffic disturbances propagate relative to a moving traffic stream.

In 1995, Bando *et al.* suggested a model that is independent of $\dot{x}_{n+1}$:

$$\ddot{x}_n(t) = \alpha[V_B(h_n(t)) - \dot{x}_n(t)] \tag{2.8}$$

where α is a constant. Here they designated V_B as some desired velocity function. This model says that what a driver really follows is some optimal velocity he/she has

in mind that depends on the front headway. For this, this model is called Optimal Velocity (OV) model. In spite of its simple form, this was a big leap towards a realistic traffic flow because it supported the formation of stop-and-go flow pattern [2, 4]. Note that OV model does not take the reaction time into consideration, so the consequence of this model implies instantaneous reaction. In 2000, Berg *et al.* also made an effort to translate a set of OV ODEs to PDE using a series expansion of the headway in terms of ρ [6]. Berg formulated

$$h\rho + \frac{h^2\partial_x\rho}{2!} + \frac{h^3\partial_{xx}\rho}{3!} + \cdots = 1 \tag{2.9}$$

by expending

$$\int_0^{h(x,t)} \rho(x+y,t)\, dy = 1 \tag{2.10}$$

in powers of y, and integrating. Keeping up to cubic terms in (2.9), expansion in a series in terms of ρ takes the following approximation:

$$h \approx \frac{1}{\rho} - \frac{\partial_x\rho}{2\rho^3} - \frac{\partial_{xx}\rho}{6\rho^4} + \frac{(\partial_x\rho)^2}{2\rho^5} + \cdots . \tag{2.11}$$

And then a continuum version was derived

$$\partial_t v + v\partial_x v = \alpha[\bar{V}(\rho) - v] + \alpha\bar{V}'(\rho)\Big[\frac{\partial_x\rho}{2\rho} + \frac{\partial_{xx}\rho}{6\rho^2} - \frac{(\partial_x\rho)^2}{2\rho^3}\Big] \tag{2.12}$$

where $\bar{V}(\rho)$ is related to V_B in a way that $\bar{V}(\rho) = V_B(1/\rho)$.

In 2001, Jiang *et al.* combined the OV model with the classical model by :

$$\ddot{x}_n(t) = \kappa[V(h_n) - \dot{x}_n(t)] + \lambda[\dot{x}_{n+1}(t) - \dot{x}_n(t)] \tag{2.13}$$

where $V(h_n)$ is some equilibrium velocity pertaining to headway, and κ and λ are sensitivity constants. This combined model supported not only the formation of stop-and-go congestion but also hysteresis loop[1] [26]. We refer to [3, 43, 44] and the references therein for the study with addition of delay time.

[1]This is a loop typically shown in speed-density plane that accounts for acceleration and deceleration branches separately.

2.2 Numerical Result

We carry out numerical experiments of (2.13) first to obtain an insight of the vehicle motions that cause inevitable instability by perturbing initial condition. With the assumption of N vehicles on a ring road, initial condition is the uniform flow with a small disturbance by one vehicle coming in (Test 1) as in Figure 2.2. To be specific, Test 1 has an initial disturbance:

$$\begin{aligned} x_n(0) &= n\tfrac{L}{N} \quad \text{for} \quad n < 50 \\ x_n(0) &= (n-\tfrac{1}{2})\tfrac{L}{N} \quad \text{for} \quad n = 50 \\ x_n(0) &= (n-1)\tfrac{L}{N} \quad \text{for} \quad n > 50 \end{aligned}$$

where L is the total length of the ring road, and $n = 1, \cdots, N+1$. This initial small perturbation can be viewed as random disturbance or consequence of lane change of $n = 50$th car. In this simulation, $L = 1500\ (m)$, $N = 100$,

$$V(h) = 6.75 + 7.91 \tanh[0.13(h-5) - 1.57] \qquad (m/s),$$

$\kappa = 0.41\ s^{-1}$, and $\lambda = 0.5\ s^{-1}$ were taken. With this choice of parameters, numerical experiments show that V is nonnegative. It, however, could go negative by varying the value of λ. For details, see hysteresis loops in [26].

Test 1 exhibits that the cars start off with decelerating because of the one car merged, and all cars experience break-acceleration-break travel at the end, see Figure 2.3. Interestingly, this also happens when one car is removed, see Test 2 in Figure 2.3. A real experiment was similarly set up and two supplementary videos can be found in [52].

In [2, 26], bifurcation study was done under linear stability analysis:

$$V'(h) < \frac{\kappa}{2} + \lambda. \tag{2.14}$$

(a) Uniform flow (b) Test 1 (c) Test 2

Figure 2.2: Uniform flow (a), disturbed flow with one entering car (b) and leaving car (c).

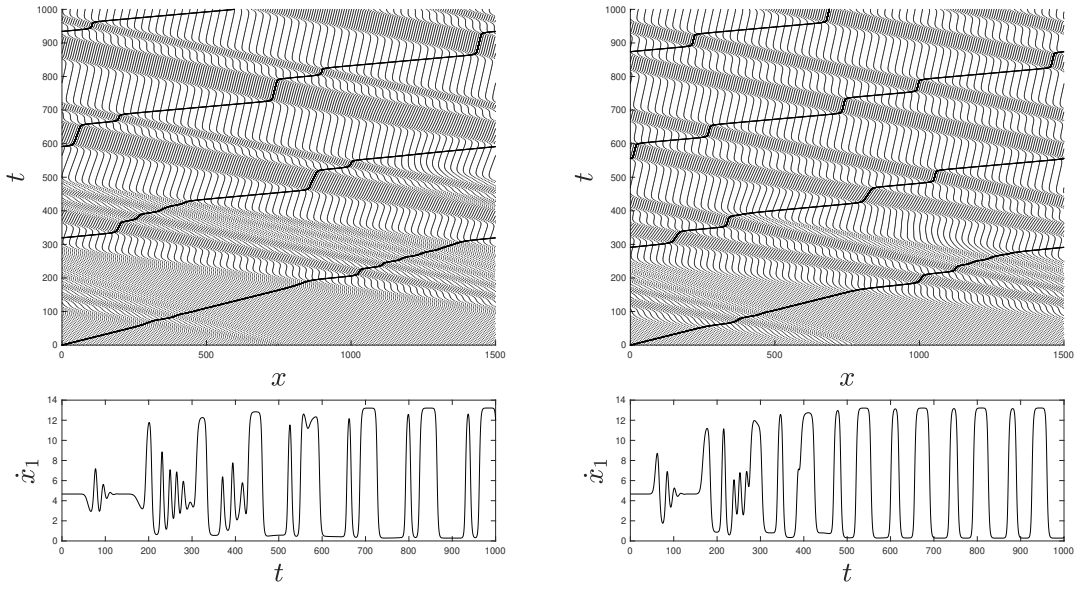

(a) Test 1: one car moving into lane, total $N+1$ vehicles (b) Test 2: one car leaving out, total $N-1$ vehicles

Figure 2.3: Top: car trajectories with #1 car trajectory (bold line). Bottom: speed of #1 car.

If (2.14) is satisfied, then small disturbance always dies out. If not, then small disturbance may result in stop-and-go formation.

From macroscopic perspective, this test indeed indicates a richness of adding the acceleration equation when modeling is concerned. Later we will take (2.13) to convert to PDE and then reproduce this stop-and-go pattern.

Closing Remarks: Microscopic approaches are, however, computationally expensive, as each vehicle has an ODE to be solved at each time step. Therefore as the number of vehicles increases, so does the size of system to be solved. For this reason, it is desirable to use the macroscopic models if a good model can be found satisfactorily.

CHAPTER III

Macroscopic Traffic Flow Model

Chapter III is concerned with macroscopic models. We begin with the scalar conservation laws of vehicles. In order for this core equation to be solvable, it requires a closure that relates mean velocity and density. A new fundamental relation is proposed. A discussion of discontinuous flux and non-convex flux is included. Then we extend to newly-developed 2x2 system model. Built on all of these, Chapter III closes with presenting two types of multilane models: scalar model (Type 1) and system model (Type 2).

3.1 Scalar Conservation Laws

In macroscopic models the interest is the collective average of traffic flow and its evolution. The underlying fundamental principle is the car mass conservation, resulting in a conservation law for the car density. In this section, we derive the mass conservation equation and discuss simple traffic examples.

3.1.1 Derivation of Equation

Consider a finite road segment $[x_1,\ x_2]$ during a time period $[t_1,\ t_2]$. Then

$$\text{total number of vehicles in } [x_1,\ x_2] \text{ at time } t = \int_{x_1}^{x_2} \rho(x,t)\ dx$$

where $0 \leq \rho \leq \rho_{max}$. ρ_{max} is the state at which vehicles are touching bumper to bumper. $\rho = 0$ implies an empty road. By dividing ρ by ρ_{max}, $0 \leq \tilde{\rho} = \frac{\rho}{\rho_{max}} \leq 1$. We drop $\tilde{}$ throughout the dissertation. Assuming that there is no on/off-ramp, the total number of vehicles in this section can change only because of traffic flowing across the boundaries x_1 or x_2:

$$\int_{x_1}^{x_2} \rho(x, t_2)\, dx = \int_{x_1}^{x_2} \rho(x, t_1)\, dx + \int_{t_1}^{t_2} \Big(\rho(x_1, t)v(x_1, t) - \rho(x_2, t)v(x_2, t)\Big)\, dt. \tag{3.1}$$

This is the integral form of conservation laws. For differentiable ρ and v, the fundamental theorem of calculus leads

$$\int_{t_1}^{t_2} \int_{x_1}^{x_2} \partial_t \rho + \partial_x(\rho v)\, dx\, dt = 0. \tag{3.2}$$

Because $x_1,\ x_2,\ t_1$ and t_2 were chosen arbitrarily, we reach a conclusion that the integrand in (3.2) vanishes, yielding the well-known LWR model (Lighthill-Whitham 1955 and Richards 1956) [37, 47]:

$$\partial_t \rho + \partial_x(\rho v) = 0. \tag{3.3}$$

This classical LWR model, a nonlinear first order PDE, treats traffic flow as a one-directional compressible fluid and studies properties induced by the interactions of vehicles as a whole.

We assume that vehicles drive at around speed limit of the road in light traffic, and slow down in increasing traffic. Therefore the average velocity of vehicles can be an a-priori relationship that describes v as a function of local ρ, $v = V(\rho)$. Depending on a variety of ways of formulating the equilibrium state velocity $V(\rho)$, this simple but insightful scalar model allows various traffic waves to arise: shocks, rarefaction waves, or compound waves. This relationship between v and ρ is, in general, called 'the speed-density relationship' in traffic flow or Fundamental diagram

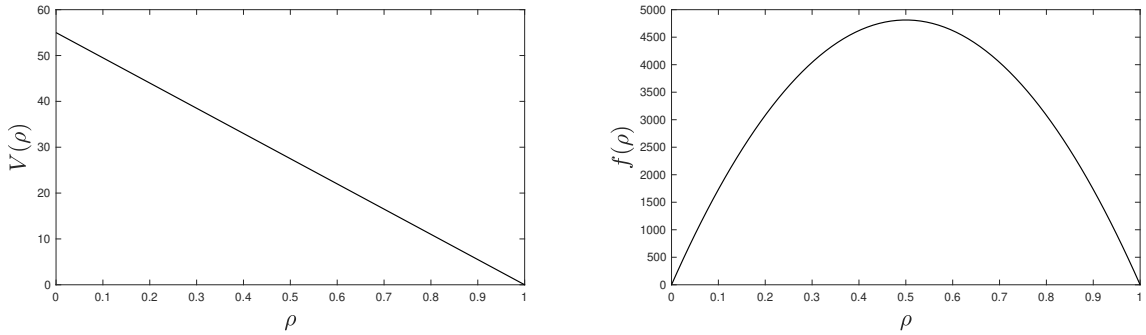

Figure 3.1: The Greenshields' model

(FD)[1] equivalently. This relation follows the general rules that v is non-increasing i.e. $V'(\rho) \leq 0$. Moreover, v tends to flatten out to zero speed when ρ approaches 1 while v stays near speed limit when ρ is very low and close to 0. The LWR model with a proper speed-density relation has been an indispensable building block since its appearance. The LWR model (3.3) with the closure relation becomes

$$\partial_t \rho + \partial_x \big(\rho V(\rho)\big) = 0. \tag{3.4}$$

A simple relationship was proposed by Greenshields *et al.* [20]:

$$V(\rho) = v_{max}(1 - \rho). \tag{3.5}$$

Together with (3.5), (3.4) is a nonlinear scalar equation. See Figure 3.1 for the speed-density relationship as well as FD of (3.5).

Closing Remarks: We close this section by revisiting simple Riemann problem associated with shock and rarefaction waves in traffic flow.

[1] In fact, FD refers to a diagram describing flux and ρ relation. Because of $f = \rho v$, speed-density relationship and FD are interchangeably used.

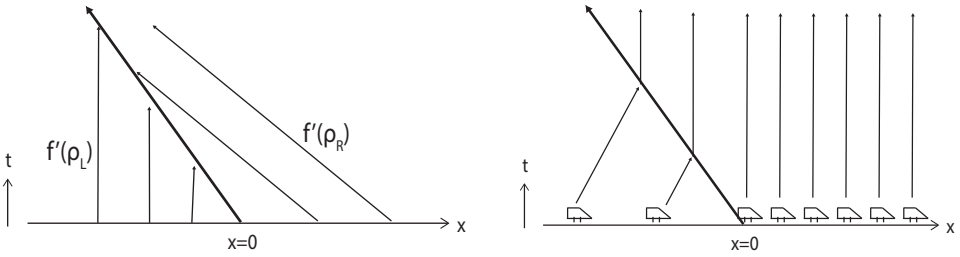

(a) Characteristics creating a shock wave (b) Visualization of vehicle trajectories

Figure 3.2: Example III.1

Example III.1. *Consider* (3.4) *with* (3.5) *with Riemann data:* $\rho_L = 0.5$ *and* $\rho_R = 1$.

This models the situation in which vehicles moving at speed $V_L > 0$ unexpectedly encounter a bumper-to-bumper traffic jam and slam on their brakes, instantaneously coming to a stop while the density jumps from ρ_L to ρ_R. We notice that characteristics in each of the regions where ρ is constant go into the shock as time evolves as in Figure 3.2a, and vehicle trajectories are shown in Figure 3.2b. Therefore, shock wave forms and propagates backwards with speed $v_{max}(1 - \rho_L - \rho_R)$. □

Example III.2. *Consider instead with* $\rho_L = 0.8$ *and* $\rho_R = 0.3$.

The vehicles to the left move initially slow but can begin to accelerate once the vehicles in front of them begin to speed up. Under the assumption of $V(\rho)$ here, each driver can speed up only by allowing the distance between her/him and the leading car to increase, and so we see a gradual acceleration and spreading out of vehicles. Vehicles are rarefied as this wave passes through, see Figure 3.3. □

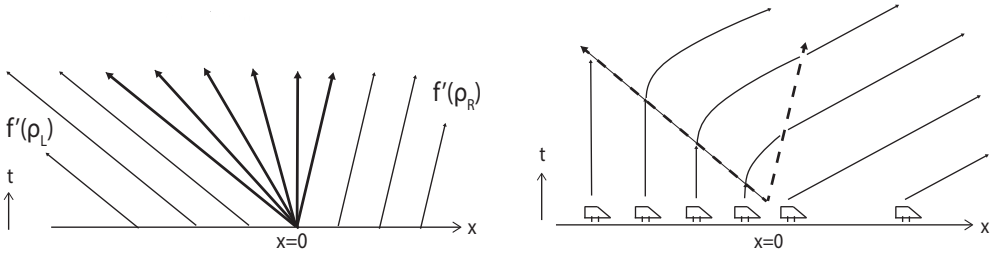

(a) Characteristics creating a rarefaction wave (b) Visualization of vehicle trajectories

Figure 3.3: Example III.2

3.1.2 Fundamental Relation and a New Fundamental Diagram

Since the earliest work measured and quantified empirically in 1930s by Greenshields *et al.* [20], there has been many studies on the relationship between flow speed and flow density due to easier access to field data, summarized in Table 3.1. A fit to the Lincoln tunnel data was found by Greenberg in 1959 [19], Underwood and Drake *et al.* proposed exponential forms separately [54, 15], and Kerner *et al.* also deployed an exponential form in their simulation [27]. Del Castillo *et al.* proposed a double exponential form [9]. Traffic flow is typically divided into two states, free flow and congested flow. Based on this, some relationships consist of two phases [57, 38]. See Figure 3.4 for a comparison. Here v_f refers to a free flow speed.

	Relationship
Greenshields *et al.* (1935)	$v_f(1-\rho)$
Greenberg (1959)	$v_f \ln(1/\rho)$
Underwood (1961)	$v_f \exp(-\rho)$
Drake *et al.* (1966)	$v_f \exp(-(\rho/3)^2/2)$
Del Castillo *et al.* (1995)	$v_f(1-\exp(1-\exp(7(1/\rho-1)/v_f)))$
Yang *et al.* (2011)	$\min\{v_f, \alpha\rho^m\}$

Table 3.1: A list of speed-density relationships.

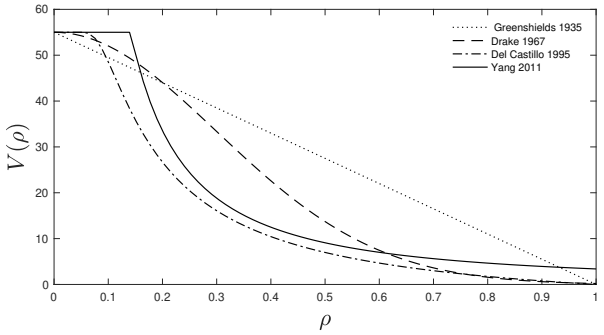

Figure 3.4: Some visual representations of Table 3.1.

We focus on the two-phase model by Yang *et al.* . The model is

$$V = \min\{v_f,\ \alpha\rho^m\} \tag{3.6}$$

where $m < 0$ and $\alpha > 0$. This model was fitted to 2009 traffic data from Interstate 95 in Virginia and α, m were optimized in [57, 11]. In congested flow, m turned out to be less than -1, which makes f turn from linear to convex as it switches from free to congested flow. One main drawback is that f in this model immediately decreases as soon as v drops down from v_f. But an observation from traffic data shows that f actually increases, albeit rather slowly even when v decreases from v_f, and then f starts to decrease as v further decreases. To capture this characteristic from the data observation, we propose a three-phase model

$$V = \min\{v_f,\ \alpha_1 \exp(\alpha_2\rho)\rho^{m_1\rho+m_2}\} \tag{3.7}$$

where $\alpha_2 \leq 0$ and $m_1 \leq 0$. Note that this has an analogous structure of (3.6), but is different in that parameters are replaced by some function of ρ, $\alpha(\rho) = \alpha_1 \exp(\alpha_2\rho)$, and m by $m(\rho) = m_1\rho + m_2$. Choice of such functions are from the data observation and this is presented in Appendix A. See Figure 3.9 for a schematic of three-phase FD. It is not easy to catch an improvement in $v - \rho$ plane, but it is noticed that in $f - \rho$ plane it fixes the drawback with this simple modification.

We take logarithm of (3.7) and reformulate the optimization problem as

$$\min_{m_1,m_2,\alpha_1,\alpha_2} \| \ln v - \ln\alpha_1 - \alpha_2\rho - m_1\rho\ln\rho - m_2\ln\rho\|_2^2$$

with $\alpha_2 \leq 0,\ m_1 \leq 0$. In Figure 3.5, the black dots associated with v are basically identical to dataset in Figure 1.6b but displayed for the FD purpose. A pair of (v, ρ) at a space and time is represented as a dot in $v - \rho$ plane, and it is aggregated over all domain in Figure 3.5. Linear regression was performed on smoothened data that

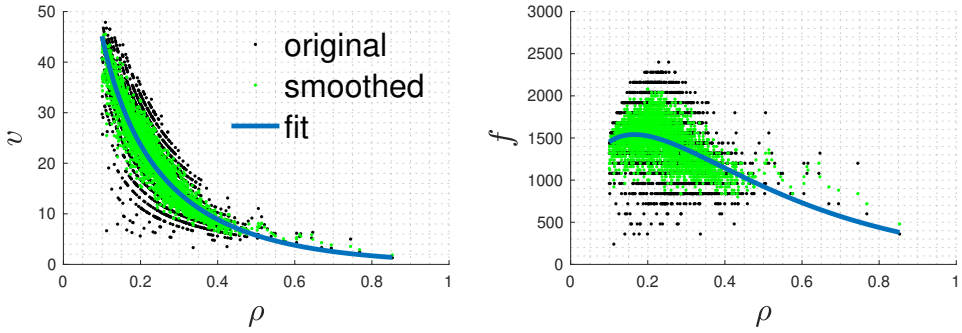

Figure 3.5: US 101 data represented in $v-\rho$ plane, original in black and smoothed data in green. Fitted curve is in blue (Left). Same data in $f-\rho$ plane (Right).

obtained by moving window with size of 4 data points and returning its mean. Recall that the US101 data was collected during peak time so there is a lack in free flow data. For this reason, we fit the congested regime only. The fit result to congested part is

$$v = 22.5 \exp(-3.3\rho)\ \rho^{0\cdot\rho-0.4}. \tag{3.8}$$

The fit (3.8) gives expected velocities and therefore the model predicts expected traffic patterns. Figure 3.5b shows the corresponding $f-\rho$ diagram. It switches from concave to decreasing convex as ρ increases. Convexity change is one of key features differing from the two-phase FD. This would have one additional increasing linear when the free flow part is completed, and this will complete a three phase FD. Having a non-convex flux in a scalar conservation laws is a completely new regime to look at, which will be addressed later. With the new three-phase results, we are capable of reconstructing the predicted mean velocity and analyzing the error[2]. Figure 3.6 reports them. In reconstruction, there are some missing data due to the lack of data availability for free flow. As two measures of performance, histogram of errors and its qq-plot describe left light long tail and right heavy tail.

[2]By error, it means predicted velocity - observed velocity.

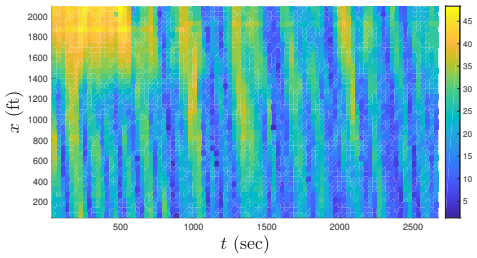

(a) Mean velocity map

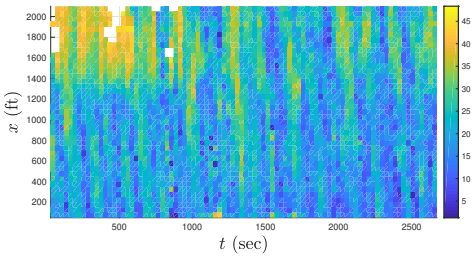

(b) Predicted mean velocity by (3.8)

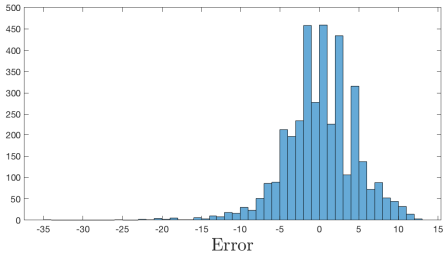

(c) Histogram of error

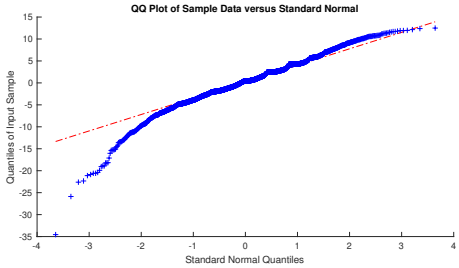

(d) Corresponding qq-plot

Figure 3.6: Reconstruction and errors of US 101

The same methodology was also performed on I-80 data. Result is below:

$$v = 20.1 \exp\left(-3.5\rho\right)\, \rho^{0\cdot\rho - 0.34}, \tag{3.9}$$

and see Figure 3.7 and 3.8.

Here we present a practical shape of the new FD, so that this can be easily tractable and applicable in PDE-based problems. For this, we constraint for FD to

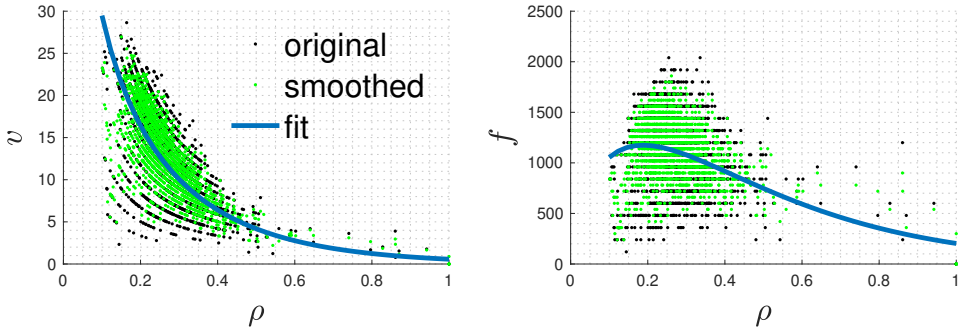

Figure 3.7: I-80 data represented in $v - \rho$ plane, original in black and smoothed data in green. Fitted curve is in blue (Left). Same data in $f - \rho$ plane (Right).

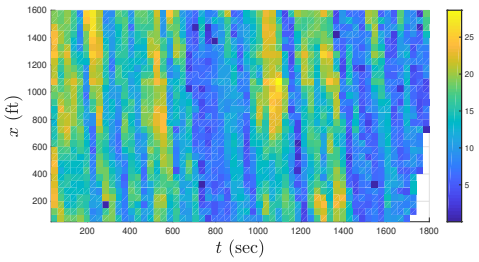

(a) Mean velocity map

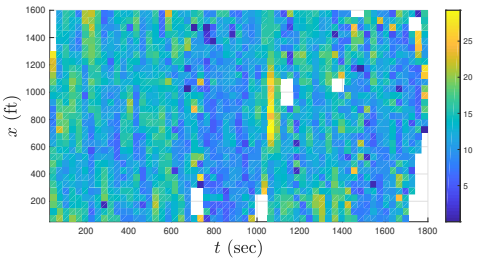

(b) Predicted mean velocity by (3.9)

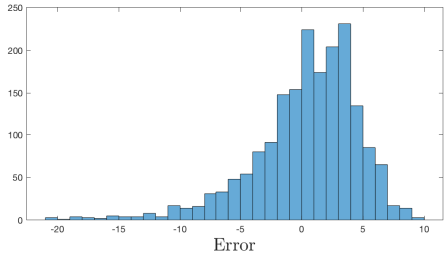

(c) Histogram of error

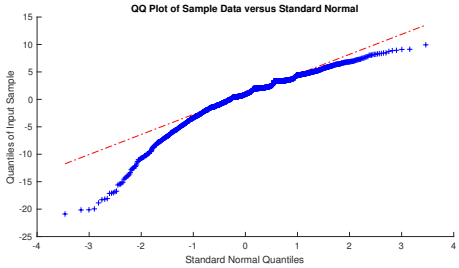

(d) Corresponding qq-plot

Figure 3.8: Reconstruction and errors of I-80

be continuous and differentiable. Assume that v_f and ρ_c[3] are provided. A posted speed limit is a good candidate, or average of max and min speed limit is another good candidate for v_f, and ρ_c usually assumed to be 10-14% of maximal density. In US101 and I-80 data, it turned out that $m_1 \approx 0$. But if we had enough data in free flow part and the transition part between free flow and congested regime, then m_1 may have played a role. Therefore in practical form, we keep m_1. Once m_1 and m_2 are determined, assigning

$$\alpha_1 = v_f \exp(-\alpha_2 \rho_c) \rho_c^{-m_1\rho_c - m_2} \quad \text{and} \quad \alpha_2 = -m_1 \log(\rho_c) - \frac{m_1\rho_c + m_2}{\rho_c}$$

will create a smooth flux function as in Figure 3.9[4]. This is an exact analogous to put constraints that

$$V(\rho_c) = v_f \quad \text{and} \quad V'(\rho_c) = 0.$$

[3] A critical density, denoted by ρ_c, is a break density point that divides a free flow and congested flow in FD.

[4] It is shifting down so that $f(\rho_{max}) = 0$ and this makes sense if we consider a static homogeneous flow in equilibrium state.

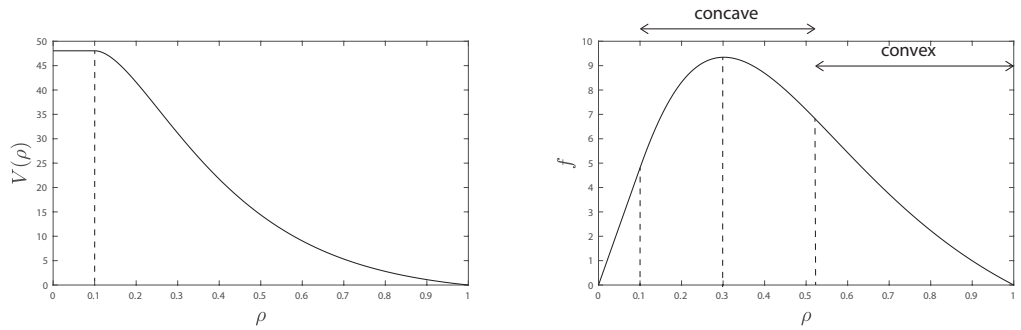

Figure 3.9: A practical shape of the new FD (3.7)

In one practical FD, $v_f = 50$, $\rho_c = 0.1$, $m_1 = -0.4$, and $m_2 = 0.4$. The maximal flux is achieved at $\rho \approx \frac{-\alpha_2 - \sqrt{\alpha_2^2 - 4m_1(m_2+1)}}{2m_1} \approx 0.30$. Observe that there are three states of traffic condition, free flow and two types of congested flow that are divided by the change in convexity nature in flux. Flux concavity changes to flux convexity at $\rho \approx 0.52$[5]. The practical form may be changed depending on different choices of parameters such as v_f, but the general shape with three phases- free, two congested in concave to convex- should remain as in Figure 3.9.

Closing Remarks: One can illustrate traffic flow under certain circumstances by constructing an appropriate form of $V(\rho)$. For night time driving example, see [34].

[5]This requires a simple algebraic calculation that needs to solve a 4th degree polynomial.

3.1.3 Riemann Problem

In this section, we discuss Riemann problems with spatially varying flux and non-convex flux, which lead to more complicated wave structure [35].

Spatially Varying Flux

It is not unusual that we encounter variable speed limit area either reduced or increased speed limit zone when driving. For instance this may be for the purpose of real-time control on the highway traffic volume, or for the specific purpose such as school zone or highways with changing surface conditions [40]. Sometimes, even the road that is unpaved or uneven forces drivers to reduce their speed. This results in average velocity of traffic that depends not only on the local density but also on the space.

Imagine that a road has a speed limit 55 mph ($x < 0$) and it drops down to 35 mph ($x > 0$), see Figure 3.10. Consider

$$\partial_t \rho + \partial_x \big(\rho V(\rho, x)\big) = 0 \tag{3.10}$$

where

$$V(\rho, x) = V_{max}(x)(1 - \rho) \tag{3.11}$$

and

$$V_{max}(x) = \begin{cases} 55, & x < 0 \\ 35, & x > 0. \end{cases} \tag{3.12}$$

Solution of the Riemann problem consists of

1. left-going and right-going waves (either shock or rarefaction wave), and
2. a stationary discontinuity at $x = 0$.

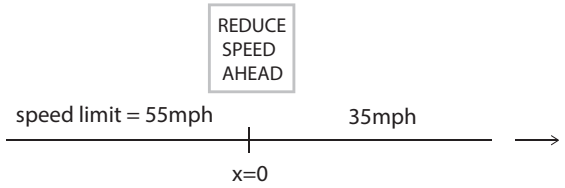

Figure 3.10: Road example of the variable speed limit

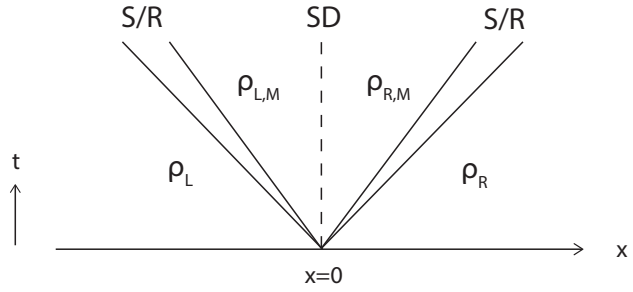

Figure 3.11: Riemann solution structure in terms of wave propagation

.

See Figure 3.11 for the solution structure. In Figure 3.11, S implies shock, R rarefaction, SD stationary discontinuity, and $\rho_{L,M}/\rho_{R,M}$ denote the intermediate states to the left/right of $x = 0$, respectively. Let us denote the flux for $x < 0$ by f_L, and for $x > 0$ by f_R. Since f_L governs the propagation of left-moving waves and f_R governs the propagation of right-moving waves, some parts of the flux curves are not admissible. The discontinuous flux is illustrated in Figure 3.12 where the locus of admissible curves are in solid curves.

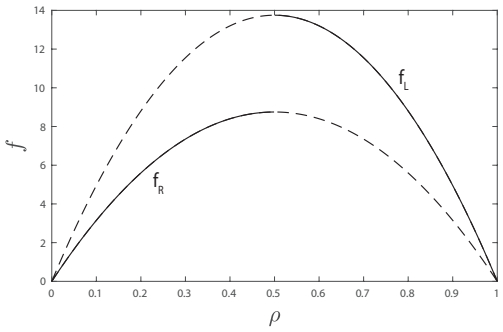

Figure 3.12: Graphs of admissible f_L and f_R in solid curves

.

Rankine-Hugoniot jump condition

$$f_L(\rho_{L,M}) - f_R(\rho_{R,M}) = s(\rho_{L,M} - \rho_{R,M})$$

across a stationary discontinuity with $s = 0$ implies that f is continuous at $x = 0$, or

$$f_L(\rho_{L,M}) = f_R(\rho_{R,M}). \tag{3.13}$$

Depending on the choice of ρ_L and ρ_R, different wave patterns may arise. We illustrate two cases below. The Riemann solution is illustrated geometrically in Figure 3.13.

Example III.3. *Solve* (3.10) *with* (3.11)*, given*

$$\rho(x,0) = \begin{cases} 0.4, & x < 0 \\ 0.3, & x > 0. \end{cases}$$

The Riemann solution contains a left-going shock from a state $\rho_L = 0.4$ to a state $\rho_{L,M} \approx 0.8$[6], with speed $\frac{f_L(\rho_L) - f_L(\rho_{L,M})}{\rho_L - \rho_{L,M}}$, a stationary jump from $\rho_{L,M} = 0.8$ to $\rho_{R,M} = 0.5$ at $x = 0$ along with a rarefaction fan from $\rho_{R,M} = 0.5$ to $\rho_R = 0.3$. The traffic slows down since the speed limit decreases at $x = 0$, and this creates a shock wave going backwards, and then gradually speeds up through a rarefaction wave. □

Example III.4. *Consider*

$$\rho(x,0) = \begin{cases} 0.9, & x < 0 \\ 0.3, & x > 0. \end{cases}$$

Then the Riemann solution contains a left-going rarefaction wave, a stationary discontinuity, and a right-going rarefaction wave. □

[6]This is one critical value satisfying $f_L(\rho) = f_R(\frac{1}{2})$.

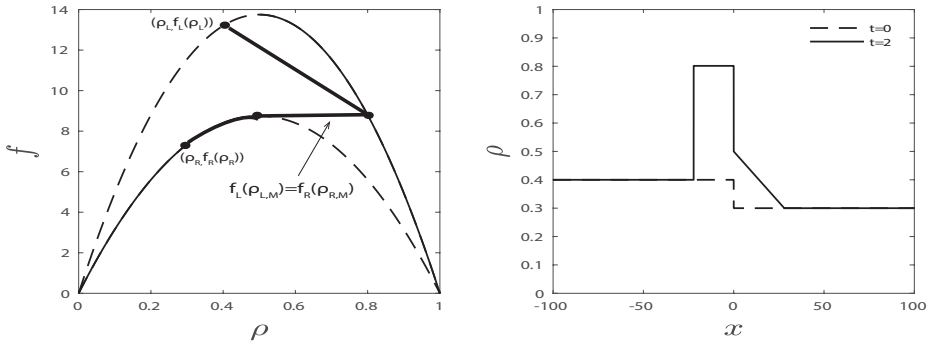

(a) Example III.3

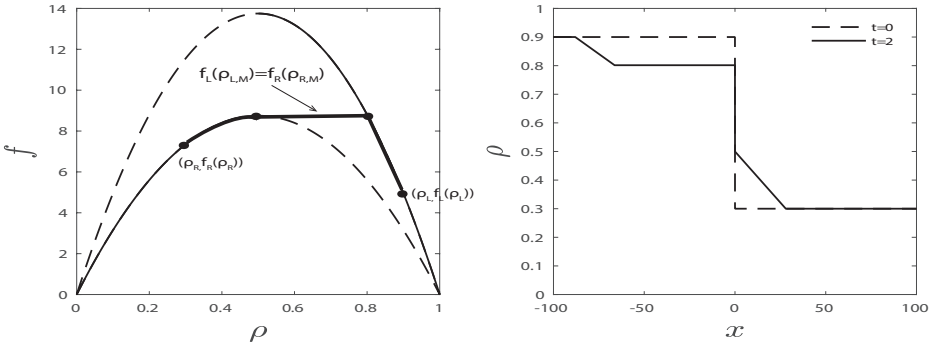

(b) Example III.4

Figure 3.13: Riemann solution locus and evolution of density.

Non-convex Flux

Recall that the data-driven three-phase flux in section 3.1.2 turned out to be non-convex with two inflection points. The solution to the Riemann problem can be determined from the graph of $f(\rho)$ by the convex-hull[7] method [35]. If $\rho_R < \rho_L$, we construct the convex hull of the set $\{(\rho, y) : \rho_R \leq \rho \leq \rho_L \text{ and } y \leq f(\rho)\}$ and look at the upper boundary of this set to determine the structure of the Riemann solution. If $\rho_L < \rho_R$, then we follow instead the convex hull of the set above the graph $y = f(\rho)$, $\{(\rho, y) : \rho_L \leq \rho \leq \rho_R \text{ and } y \geq f(\rho)\}$, and read off the lower boundary of this set. Note that if $f(\rho)$ is convex (or concave), then the convex hull construction gives either a single shock or a single rarefaction as we expected. Let us take a look at

[7]The convex hull is defined as the smallest convex set containing the original set.

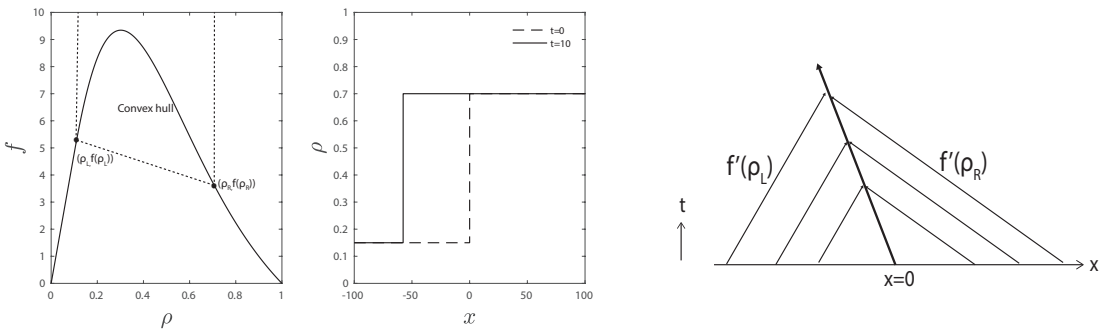

(a) Example III.5 (b) Characteristics

Figure 3.14: Convex hull, evolution of density, and characteristics of Example III.5

two examples to seek for Riemann solution by constructing convex hull.

Example III.5. *Solve*

$$\partial_t \rho + \partial_x f(\rho) = 0 \tag{3.14}$$

with

$$\rho(x,0) = \begin{cases} 0.15, & x < 0 \\ 0.7, & x > 0 \end{cases}$$

where $f(\rho)$ is the three-phase FD in Figure 3.9.

By constructing the convex hull, it is composed of a straight line segment from $(\rho_L, f(\rho_L))$ to $(\rho_R, f(\rho_R))$, see Figure 3.14a. The straight line represents a shock jumping from ρ_L to ρ_R. Therefore, the Riemann solution contains a shock wave going backwards, see Figure 3.14a and its corresponding characteristics in b. □

Example III.6. *Consider*

$$\rho(x,0) = \begin{cases} 0.7 & x < 0 \\ 0.15, & x > 0. \end{cases}$$

By constructing the convex hull, it follows from $(\rho_R, f(\rho_R)$ to $(\rho^*, f(\rho^*))$ and then has a straight line segment down to $(\rho_L, f(\rho_L))$, see Figure 3.15a. The segment where

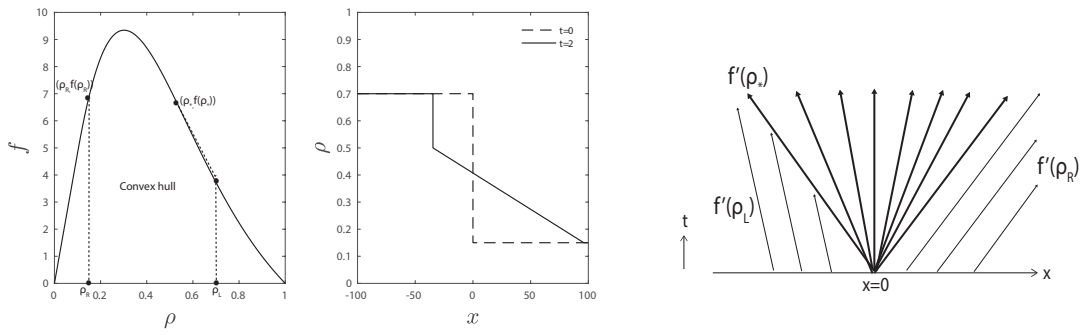

(a) Example 6 (b) Characteristics

Figure 3.15: Convex hull, evolution of density, and characteristics of Example III.6

boundary follows is the rarefaction wave and the straight line is a shock jumping from $\rho = \rho^*$ to $\rho = \rho_L$, where ρ^* is the inflection point. Hence, the Riemann solution contains a shock wave propagating to the left followed by a rarefaction, see Figure 3.15a, as a compound wave. Figure 3.15b is its characteristics. □

Example III.7. *Consider*

$$\rho(x,0) = \begin{cases} 0.8, & x < 0 \\ 0.7, & x > 0 \end{cases}$$

Both states are in a very congested flow and $\rho_L = 0.8 > \rho_R = 0.7$. In this case, we end up having a Riemann solution with a shock traveling to the left. This is the entropy-satisfying solution that makes sense mathematically, however we would expect a rarefaction fan in reality. This will always happen if flux has the convex portion. □

Closing Remarks: Variations to scalar model do exist. Appropriate source terms can be put into model to investigate, for example, on/off-ramps effects [35]. Adding a source term to capture the stochastic nature of traffic is another way of approach [57]. Some generalizations of scalar models will briefly follow.

3.1.4 Generalization

One generalization based on LWR model is to consider different types of vehicles known as multi-class or n-population. Heterogeneous vehicles' characters are reflected in that automobiles allow a higher speed limit than trucks, and that the length of automobiles is smaller than that of trucks, etc [56, 58, 5]. Let us take a look one model of 2-population in [5]

$$\partial_t \rho_i + \partial_x(\rho_i v_i) = 0 \quad \text{for} \quad i = 1,\ 2 \tag{3.15}$$

where ρ_i is the density of vehicles belonging to the ith class. $v_i = v_i(r) = V_i\Big(1 - \frac{r}{r_{max}}\Big)$ where $r = l_1\rho_1 + l_2\rho_2$, l_i is the average length of vehicles in ith class, and V_i is maximal speed of class i. Assuming $l_i = 1$ for $i = 1, 2$ and $r_{max} = 1$, (3.15) becomes

$$\partial_t \rho_i + \partial_x\Big(\rho_i V_i(1 - \sum_{j=1}^{2} \rho_j)\Big) = 0 \quad \text{for} \quad i = 1,\ 2. \tag{3.16}$$

This can also viewed as using 'weighted maximal speed' as follows

$$\partial_t \rho + \partial_x(\rho V_m(1 - \rho)) = 0 \tag{3.17}$$

where $V_m = \frac{\rho_1}{\rho} V_1 + \frac{\rho_2}{\rho} V_2$ and $\rho = \rho_1 + \rho_2$. It has an analogous form as (3.4) but has weighed elements in V_m. In [56], they developed another 2-population model in which numerical simulations showed two-capacity regimes, hysteresis and platoon dispersion. The idea in [58] is that the performance of vehicles belonging to different classes is different in free flow[8] but indistinguishable in heavy traffic [9].

Another generalization is to consider flow of traffic over more than a single lane. This can be done by introducing a road configuration $n(x)$ to indicate the number of lanes and consider the lane-aggregate model

$$\partial_t\big(n(x)\rho\big) + \partial_x\big(n(x)\rho V(\rho)\big) = 0 \tag{3.18}$$

[8] This is mainly due to the fact that V_m for automobiles is greater than that for trucks.
[9] Both type of vehicles travel at the same group speed

with ρ the average lane car density across n lanes. Varying $n(x)$, one may simulate lane closure or open-up [33].

Closing Remarks: Despite of variations in LWR model, scalar conservation laws alone fails to explain complicated realistic phenomena, such as stop-and-go oscillations [36].

3.2 System

In the LWR model, $v = V(\rho)$ implies that velocity adjusts instantaneously to density. This is clearly an over simplification. Vehicles react to flow conditions, they accelerate or decelerate in response to traffic flow around them, possibly in consideration of vehicle mechanical constraints. The LWR model cannot describe these processes. In recent years, higher-order models[10] have been proposed that treat velocity $v = v(x,t)$ as a separate dependent variable and describes acceleration, response time etc.

3.2.1 Literature Review

There are numerous 2x2 systems: some are inspired by gas dynamics and others are derived from the microscopic acceleration equation [46, 55, 27, 1, 6, 12, 25, 59]. Payne in 1971 and Whitham in 1974 (PW) [46, 55] first proposed a model inspired by gas dynamics

$$\begin{aligned} \partial_t \rho + \partial_x(\rho v) &= 0 \\ \partial_t v + v\partial_x v &= \tfrac{V(\rho)-v}{T} - \tfrac{P'(\rho)\partial_x \rho}{\rho} \end{aligned} \tag{3.19}$$

where the acceleration is a summation of relaxation term and pressure term. Here T is the relaxation time that takes to relax to some equilibrium velocity $V(\rho)$. By

[10] From a mathematical point of view, it means 'a system of two-(or three-) equation models' rather than 'second-(or high-) order models'. By convention these models are sometimes referred to as high-order models.

convention, $V(\rho)$ can be replaced by one choice among many in section 3.1.2. $P(\rho)$ is a pressure[11] satisfying $P(\rho) = \rho^\gamma$, $\gamma > 0$. The PW model couples velocity dynamics as a second equation in order to link ρ and v, viewing them as independent variables. It is worthwhile to point out that the speed-density relation, $V(\rho)$, plays a part even in 2x2 system, and this re-emphasize the importance of its study. The properties of the system are controlled by the eigenvalues of the system. These eigenvalues, also known as characteristic speeds, determine how traffic information is propagated in the stream. It turns out that

$$\lambda_1 = v - \sqrt{P'(\rho)} < \lambda_2 = v + \sqrt{P'(\rho)}.$$

We note that the second eigenvalue is greater than the traffic velocity v. It means that some part of the information travels faster than average flow speed. As a result, waves associated with the second characteristic always reach vehicles from 'behind'. This happens in fluid dynamics but is an unrealistic property to traffic. A driver is an anisotropic particle that responds to frontal stimuli as opposed to the fact that a fluid particle may respond to stimuli both from the front and behind. It also turned out that PW model may produce negative travel velocity, i.e. wrong-way travel [14].

In 2000, Aw and Rascle (AR) proposed a new system to address these drawbacks by simply replacing the space derivative with the convective derivative [1]. Replacing $\partial_x(P(\rho))$ by $\rho(\partial_t + v\partial_x)P(\rho)$ in (3.19) leads to AR model ignoring the relaxation term:

$$\begin{aligned} \partial_t \rho + \partial_x(\rho v) &= 0 \\ \partial_t(v + P(\rho)) + v\partial_x(v + P(\rho)) &= 0 \end{aligned} \tag{3.20}$$

where $P(\rho) = \rho^\gamma$, $\gamma > 0$, is an increasing function. They proposed five traffic model principles including so-called Anisotropy condition that prevents rare disturbances

[11] In physics, pressure depends on Newton's second law of motion because a difference in pressure across a surface implies a difference in force, which can result in an acceleration, if there is no additional force to balance it.

from propagating forward. This is a condition that eigenvalues of the system are at most the traffic velocity v

$$\lambda \leq v.$$

With a choice of $P(\rho)$ above, AR model ensures the anisotropic property:

$$\lambda_1 = v - \rho P'(\rho) \ < \ \lambda_2 = v.$$

Therefore, every driver reacts to what happens in front and is not affected by disturbance from behind. Qualitative properties that braking/accelerating produces shock/rarefaction waves is also one of principles, which will be discussed later.

Around the same period, independently, Zhang proposed a model in 2002 [59]:

$$\begin{aligned} \partial_t \rho + \partial_x(\rho v) &= 0 \\ \partial_t v + (v + \rho V'(\rho))\partial_x v &= 0. \end{aligned} \tag{3.21}$$

A micro-to-macro link is established for this model, meaning that the second equation is derived from the microscopic car-following model (2.6), which naturally carries the anisotropic property: $v + \rho V'(\rho) = \lambda_1 \ < \ \lambda_2 = v$.

Closing Remarks: To derive the macroscopic acceleration equation, vehicle-level models should guide us a reasonably correct way. First of all, traffic flow is not really the physics as in gas dynamics. It is difficult to interpret pressure (or pressure-like term) in traffic flow. Second of all, microscopic acceleration model (2.13) can reproduce realistic flow patterns such as the appearance of stop-and-go pattern. Existing 2x2 systems have the general form

$$\begin{aligned} &\partial_t \rho + \partial_x(\rho v) = 0 \\ &\partial_t v + v\partial_x v = \underbrace{\tfrac{V(\rho)-v}{T}}_{\text{relaxation term}} + \underbrace{\cdots}_{\text{reaction terms}}. \end{aligned} \tag{3.22}$$

Different models can be formulated for the acceleration equation depending on descriptions towards reaction term from different routes. Recall that Example III.7 produced an opposite formation of wave to what was expected due to the convex part. In 2x2 system, there would be no issue using the convex FD.

3.2.2 A New Model

Microscopic car-following model (2.13) governs the dynamic of each vehicles' positions and velocities in a way that it depends on the headway and the relative speed. First our goal is to embed this idea into the macroscopic level. We assume that all drivers react in a standard way. To transform vehicle acceleration equation (2.13) to macroscopic level, we introduce macroscopic variable $v(x,t)$ that is smooth. Then define $v(x_n(t),t) = \dot{x}_n(t)$ and $v(x_n(t)+h(t),t) = \dot{x}_{n+1}(t)$ where $h(t) = x_{n+1}(t) - x_n(t)$. We then expand

$$\dot{x}_{n+1}(t) - \dot{x}_n(t) = v(x_n(t)+h(t),t) - v(x_n(t),t) = h\partial_x v + \frac{h^2}{2}\partial_{xx} v + \frac{h^3}{6}\partial_{xxx} v + ...$$

and truncate the expansion ignoring cubic terms to yield the so-called non-equilibrium model

$$\partial_t v + v\partial_x v \approx \frac{V(\rho) - v}{T} + \frac{h}{\tau}\partial_x v + \frac{h^2}{2\tau}\partial_{xx} v. \tag{3.23}$$

Here $V(\rho)$ is an optimal velocity function, T is a relaxation time and τ a reaction time.

We denote by s the *Space* between vehicles, that is the distance between the front bumper of one vehicle to the rear bumper of the vehicle ahead of it, and by h the *Headway*, that is the distance from front bumper to front bumper. We therefore have, $h = s + l_c$ where l_c is the car length. See Fig. 3.16a. We further assume that there is a minimal safety space between vehicles at which the vehicles will come to a

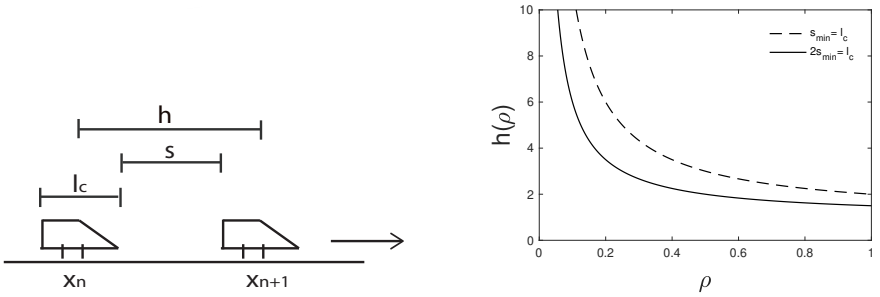

(a) Headway and its relations (b) Headway function of density

Figure 3.16: Headway in microscopic (a) and macroscopic (b) description

standstill, and denote this distance by s_{min} (for example, a certain fraction of a car length). We relate microscopic headway to macroscopic density as follows

$$h(\rho) = \frac{s_{\min}}{\rho} + l_c. \tag{3.24}$$

Putting (3.23) together with the conservation of car density leads to the viscous 2x2 system

$$\begin{aligned} \partial_t \rho + \partial_x(\rho v) &= 0 \\ \partial_t v + (v - \frac{h(\rho)}{\tau})\partial_x v &= \frac{V(\rho) - v}{T} + \frac{h^2(\rho)\partial_{xx} v}{2\tau}. \end{aligned} \tag{3.25}$$

(3.25) satisfies the anisotropy condition:

$$\lambda_1 = v - \frac{h(\rho)}{\tau} < \lambda_2 = v.$$

No information travels faster than the average traffic velocity. Moreover,

$$\nabla\lambda_1 \cdot r_1 < 0 \text{ and } \nabla\lambda_2 \cdot r_2 = 0$$

where r_i are eigenvectors

$$r_1 = \begin{pmatrix} 1 \\ -\frac{h(\rho)}{\tau\rho} \end{pmatrix}, \qquad r_2 = \begin{pmatrix} 1 \\ 0 \end{pmatrix}$$

corresponding to λ_i for $i = 1, 2$. The first condition, genuinely nonlinear field, satisfies the property that flow deceleration leads to shock waves (converging characteristics)

and flow acceleration gives rise to rarefaction waves (diverging characteristics). The second condition, linearly degenerate field, is associated with contact discontinuity, in the context of traffic flow it describes density change carried with average car speed.

Non-conservative system

The second equation in (3.25) describes the rules governing car acceleration and does not reflect a conservation law. Acceleration is the natural quantity to use to describe the traffic flow dynamics, yet as a consequence, the resulting 2x2 system is not in conservation form. Clearly, the left-hand side of (3.25) by itself, being in non-conservation form, is not valid to predict flow patterns involving shock waves. We also note that the right-hand side of (3.25) includes two terms: a relaxation term and a diffusion term. We have conducted numerical simulations of (3.25) including both relaxation and diffusion terms, and compared them to simulations with the relaxation term alone. In Figure 3.17, we present numerical Riemann solution for three cases: hyperbolic system itself, denoted by 0 RHS, hyperbolic system with relaxation term, Relaxed RHS, and hyperbolic system with relaxation and diffusion terms, Relaxed + Viscous RHS. We concluded that the 'hyperbolic' solution is substantially modified by the inclusion of the relaxation term, but once relaxation is included, the diffusion has only a negligible effect on the solution, and may often be dropped. The model we propose is therefore

$$\begin{aligned} \partial_t \rho + \partial_x(\rho v) &= 0 \\ \partial_t v + (v - \frac{h(\rho)}{\tau})\partial_x v &= \frac{V(\rho) - v}{T} \end{aligned} \tag{3.26}$$

where $\frac{h(\rho)}{\tau}$ is the speed of propagation of small disturbance mostly due to the response explained by the relative speed between cars.

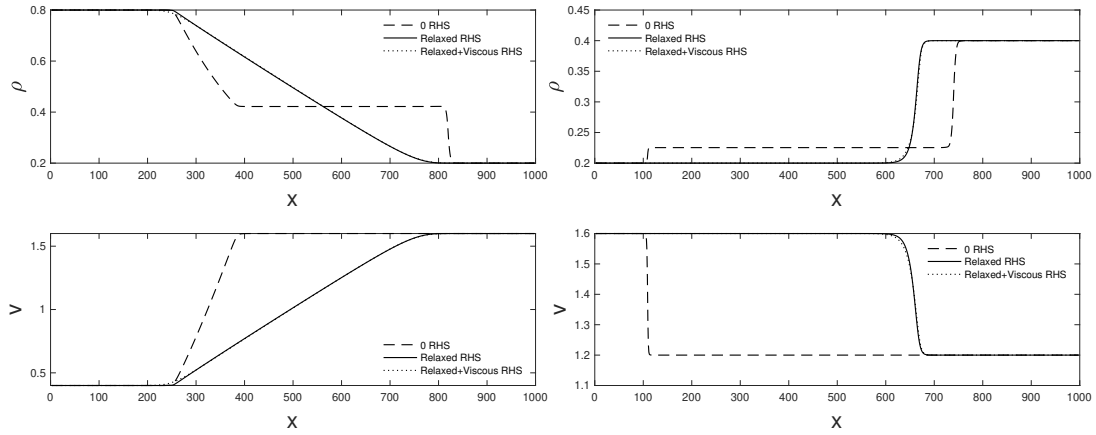

(a) Initial $\rho_L > \rho_R$ (b) Initial $\rho_L < \rho_R$

Figure 3.17: Numerical study on diffusive effect

3.3 New Multilane Models

In this section we generalize single lane models to multilane, we formulate lane changing conditions and incorporate inter lane exchange terms. We propose two types of a multilane model: the first consists of only mass conservations referred to as Type 1, and the other is in a form of systems, based on the new 2x2 system (3.26), referred to as Type 2. Other multilane models were studied in [39, 22, 23, 29, 24, 30, 21]. We assume that

1. We consider only one vehicle class whose length is l_c. $s_{\min}$ can be assumed to be constant provided one class of vehicle is considered. Note, however, that it may vary when multi-class plays a role. For example, trucks require larger $s_{\min}$ than automobiles.

2. ρ_i is the density in lane i for $i = 1, \cdots, n$.

3. $V(\rho_i)$ is the optimal velocity in lane i that is a given function of ρ_i while v_i is the average velocity that is independent of the surrounding ρ_i.

3.3.1 Lane Change Conditions

We assume that from a driver's standpoint, lane switch from lane i to a target lane j (either $i-1$ or $i+1$) is oftentimes triggered if an extra speed is gained. This first condition can be formulated by

$$v_j > (1+\alpha)v_i \tag{3.27}$$

where $\alpha \in [0,\ 1]$ that tends to be relatively small. Note that v_i should be regarded as $V(\rho_i)$ in scalar models. (3.27) says that one gains at least $\alpha\%$ of current speed v_i by switching to lane j. Once this necessary incentive is met, drivers' decision to switch lanes is prompted by checking a sufficient factor: whether or not there is enough headway (or empty space) in lane j for oneself to merge in. With (3.24), the second lane change condition now may be expressed as

$$h(\rho_j) > h_{\min} + v_i\tau_{lc}. \tag{3.28}$$

τ_{lc} is a time that takes for changing lanes. The right-hand side in (3.28) expresses the physical distance to merge for a driver traveling at v_i. It consists of the minimal headway that is required even with $v_i = 0$ plus $v_i\tau_{lc}$ that is a distance to complete the change. (3.28) says that the current headway in target lane j, $h(\rho_j)$, has to be strictly larger than the required distance. τ_{lc} is assumed to be constant in this work, but this can be generalized more. For example, defensive drivers with speed v_i, who would require larger τ_{lc}, are likely to need more distance than aggressive drivers. This way, τ_{lc} could depend on drivers' characteristics, or could depend on velocity. This linear assumption in v_i can also be found in the reaction thresholds in [29], [28].

When considering three lanes or more, the priority order of lane change in the middle lane is designated as follows: when a driver needs to speed up, the person

attempts toward the left lane first. If a driver finds a spot, then the driver will switch the lane. However, if this cannot be conducted because either of lane change condition is not satisfied, the person then attempts to the right. One would stay its lane if changing to the right lane is not even allowed.

Closing Remarks: With the two lane change conditions in mind, we now first generalize LWR model to multilane model. For this, we extend the idea of single mass conservation into n mass conservations in which each equation represents the flow in each lane, coupled through source terms representing gain or loss of inter-lanes due to lane switches.

3.3.2 Multilane Scalar and System Models

Multilane Scalar Model (Type 1)

In Type 1, we essentially have n mass conservations regarding each lane for each conserved quantity, ρ_i for $i = 1, \cdots, n$. ρ_i is then coupled through source terms representing mass gain or loss by lane changes. It takes the form

$$\partial_t \rho_i + \partial_x\big(\rho_i V(\rho_i)\big) = \text{Loss}_i + \text{Gain}_i \tag{3.29}$$

where

$$\text{Loss}_i = -\frac{s_{i,i-1} + s_{i,i+1}}{\tau_{lc}} R\rho_i \tag{3.30a}$$

$$\text{Gain}_i = \frac{s_{i-1,i}}{\tau_{lc}} R\rho_{i-1} + \frac{s_{i+1,i}}{\tau_{lc}} R\rho_{i+1} \tag{3.30b}$$

for $i = 1, \cdots, n$. This is a hyperbolic set of balance laws. Here $\rho_0 = \rho_{n+1} = 0$. Loss and gain involve mass exchanges only when lane change happens. Even when lane change conditions are met, not all drivers may choose to switch lanes. For this, we use R to denote the fraction of drivers that may choose to switch. τ_{lc} is the time for

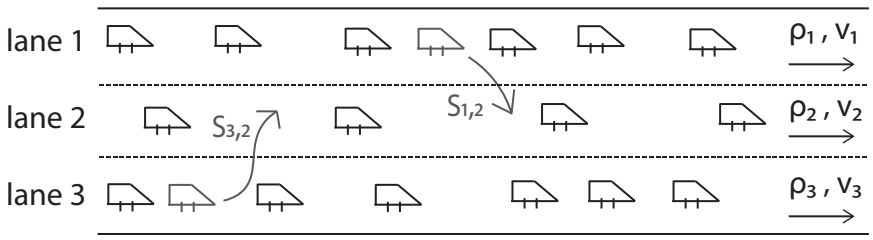

Figure 3.18: Diagram illustrating lane changes in three lanes

changing lanes and $s_{i,j}$ is

$$s_{i,j} = \begin{cases} 1 & \text{if} \quad \begin{cases} V(\rho_j) > (1+\alpha)V(\rho_i) \\ h(\rho_j) > h_{\min} + V(\rho_i)\tau_{lc} \end{cases} \\ 0 & \text{otherwise} \end{cases}$$

$s_{i,j}$ is an indicator function of lane-changing. $s_{i,j}$ may be expressed concisely as

$$\max\Big\{\ 0,\ \min\big\{\ \text{sign}(V(\rho_j) - (1+\alpha)V(\rho_i),\ \text{sign}(h(\rho_j) - h_{\min} - V(\rho_i)\tau_{lc})\ \big\}\Big\}.$$

See Figure 3.18 for a three lanes schematic. In the simulations in this work, R is constant for simplicity. Note that $s_{0,1} = s_{1,0} = s_{n+1,n} = s_{n,n+1} = 0$. Switching on and off the source terms in (3.29), we are capable of differentiating the effect of lane changes. Also the fact that summing up over all lanes results in zero source tells that there is a conservation over all lanes but not in-between lanes because of lane switches. We also deal with effects of parameters (l_c, $s_{\min}$, τ_{lc}, etc) when we visit section 4.2. Three-lane example is following

$$\begin{aligned} \partial_t\rho_1 + \partial_x\big(\rho_1 V(\rho_1)\big) &= -\frac{s_{1,2}}{\tau_{lc}}R\rho_1 + \frac{s_{2,1}}{\tau_{lc}}R\rho_2 \\ \partial_t\rho_2 + \partial_x\big(\rho_2 V(\rho_2)\big) &= \frac{s_{1,2}}{\tau_{lc}}R\rho_1 - \frac{s_{2,1}+s_{2,3}}{\tau_{lc}}R\rho_2 + \frac{s_{3,2}}{\tau_{lc}}R\rho_3 \\ \partial_t\rho_3 + \partial_x\big(\rho_3 V(\rho_3)\big) &= -\frac{s_{3,2}}{\tau_{lc}}R\rho_3 + \frac{s_{2,3}}{\tau_{lc}}R\rho_2. \end{aligned} \tag{3.31}$$

Recall that $V(\rho_i)$ in Type 1 locally depends on nearby ρ_i. Oftentimes, the average speed in real traffic does not reflect ρ explicitly. We now build up the Type 2 multilane model based on the 2x2 system that considers this element.

Multilane System Model (Type 2)

Including the lane changing wisdom in the same way, we extend the single-lane 2x2 system to multilane:

$$\partial_t \rho_i + \partial_x\big(\rho_i v_i\big) = \text{Loss}_i + \text{Gain}_i \tag{3.32a}$$

$$\partial_t v_i + (v_i - \frac{h(\rho_i)}{\tau})\partial_x v_i = \frac{V(\rho_i) - v_i}{T} + \frac{s_{i-1,i}}{\tau_{lc}} R\frac{\rho_{i-1}}{\rho_i}(v_{i-1} - v_i) + \frac{s_{i+1,i}}{\tau_{lc}} R\frac{\rho_{i+1}}{\rho_i}(v_{i+1} - v_i). \tag{3.32b}$$

$v_0 = v_{n+1} = 0$. In (3.32b), there are reaction terms associated with intra-lane acceleration: one is acceleration towards an equilibrium speed and the other is an approximate acceleration towards the speed of car ahead. And the exchange terms involving $(v_i - v_j)$ are inter-lane acceleration towards the speed in the target lane due to the lane changing. If a car in the other lane with a slower speed moves into the target lane, it causes some deceleration. This way v's in different lanes are allowed to communicate each other through this term as far as lane change is concerned. For a three-lane example, this reads

(3.33)

$$\begin{aligned}
\partial_t \rho_1 + \partial_x(\rho_1 v_1) &= -\frac{s_{1,2}}{\tau_{lc}} R\rho_1 + \frac{s_{2,1}}{\tau_{lc}} R\rho_2 \\
\partial_t v_1 + (v_1 - \frac{h(\rho_1)}{\tau})\partial_x v_1 &= \frac{V(\rho_1) - v_1}{T} + \frac{s_{2,1}}{\tau_{lc}} R\frac{\rho_2}{\rho_1}(v_2 - v_1) \\
\partial_t \rho_2 + \partial_x(\rho_2 v_2) &= \frac{s_{1,2}}{\tau_{lc}} R\rho_1 - \frac{s_{2,1} + s_{2,3}}{\tau_{lc}} R\rho_2 + \frac{s_{3,2}}{\tau_{lc}} R\rho_3 \\
\partial_t v_2 + (v_2 - \frac{h(\rho_2)}{\tau})\partial_x v_2 &= \frac{V(\rho_2) - v_2}{T} + \frac{s_{1,2}}{\tau_{lc}} R\frac{\rho_1}{\rho_2}(v_1 - v_2) + \frac{s_{3,2}}{\tau_{lc}} R\frac{\rho_3}{\rho_2}(v_3 - v_2) \\
\partial_t \rho_3 + \partial_x(\rho_3 v_3) &= \frac{s_{2,3}}{\tau_{lc}} R\rho_2 - \frac{s_{3,2}}{\tau_{lc}} R\rho_3 \\
\partial_t v_3 + (v_3 - \frac{h(\rho_3)}{\tau})\partial_x v_3 &= \frac{V(\rho_3) - v_3}{T} + \frac{s_{2,3}}{\tau_{lc}} R\frac{\rho_2}{\rho_3}(v_2 - v_3).
\end{aligned}$$

Multilane model with more than three lanes can be formulated as desired.

Closing Remarks: Multilane model especially benefit from understanding traffic bottleneck. Recall that chronic traffic bottleneck occurs most of the time in the cases of lane-closing, accidents, ramps etc, where it seems that the multilane model should play a role. Studying lane-by-lane traffic flow capturing lane switch effects also provides us a more accurate understanding of overall traffic behavior.

CHAPTER IV

Numerical Method and Result

Chapter IV includes numerical methods and PDE-based computations built on Chapter III.

4.1 Numerical Method Revisit

Upwind Scheme Revisit

Consider 2x2 model (3.26) in matrix form

$$\partial_t W + A(W)\partial_x W = S(W)$$

where

$$W = \begin{pmatrix} \rho \\ v \end{pmatrix},\ A(W) = \begin{pmatrix} v & \rho \\ 0 & v - \frac{h(\rho)}{\tau} \end{pmatrix},\ \text{and } S(W) = \begin{pmatrix} 0 \\ \frac{V(\rho)-v}{T} \end{pmatrix}.$$

The eigenstructure is given by the matrices

$$R = \begin{pmatrix} 1 & 1 \\ -\frac{h(\rho)}{\tau\rho} & 0 \end{pmatrix} \text{ and } \Lambda = \begin{pmatrix} v - \frac{h(\rho)}{\tau} & 0 \\ 0 & v \end{pmatrix}$$

so that $A(W)R = R\Lambda$. We use a Roe-type upwind scheme with the source term by projecting $S(W)$ onto the eigenvectors of $A(W)$ as illustrated in section 1.1.2. $A(W)$ is linearized about averages at the cell interface

$$\bar{\rho} = \frac{\rho_{i+1} + \rho_i}{2},\ \bar{v} = \frac{v_{i+1} + v_i}{2}.$$

The source term is approximated by

$$\bar{S} = \frac{S_{i+1} + S_i}{2}.$$

Wave strengths are then

$$\begin{aligned} \alpha_1 &= \tfrac{\tau\bar{\rho}\Delta v}{-h(\bar{\rho})}, \quad \alpha_2 = \Delta\rho - \alpha_1 \\ \beta_1 &= \tfrac{\tau\bar{\rho}S_2}{-h(\bar{\rho})}, \quad \beta_2 = -\beta_1 \end{aligned}$$

where $\Delta(\ ) = (\ )_{i+1} - (\ )_i$. This scheme can be also applicable to Type 1 and 2 models. For example, the three lane model of Type 2 (3.33) has eigenstructure

$$R = \begin{pmatrix} 1 & 1 & 0 & 0 & 0 & 0 \\ -\frac{h(\rho_1)}{\tau\rho_1} & 0 & 0 & 0 & 0 & 0 \\ 0 & 0 & 1 & 1 & 0 & 0 \\ 0 & 0 & -\frac{h(\rho_2)}{\tau\rho_2} & 0 & 0 & 0 \\ 0 & 0 & 0 & 0 & 1 & 1 \\ 0 & 0 & 0 & 0 & -\frac{h(\rho_3)}{\tau\rho_3} & 0 \end{pmatrix}$$

and

$$\Lambda = \mathrm{diag}\Big(v_1 - \frac{h(\rho_1)}{\tau},\ v_1,\ v_2 - \frac{h(\rho_2)}{\tau},\ v_2,\ v_3 - \frac{h(\rho_3)}{\tau},\ v_3\Big).$$

Wave strengths are

$$\begin{aligned} \alpha_1 &= \tfrac{\tau\bar{\rho}_1\Delta v_1}{-h(\bar{\rho}_1)}, \quad \alpha_2 = \Delta\rho_1 - \alpha_1, \quad \alpha_3 = \tfrac{\tau\bar{\rho}_2\Delta v_2}{-h(\bar{\rho}_2)} \\ \alpha_4 &= \Delta\rho_2 - \alpha_3, \quad \alpha_5 = \tfrac{\tau\bar{\rho}_3\Delta v_3}{-h(\bar{\rho}_3)}, \quad \alpha_6 = \Delta\rho_3 - \alpha_5 \end{aligned}$$

$$\begin{aligned} \beta_1 &= \tfrac{\tau\bar{\rho}_1\bar{S}_2}{-h(\bar{\rho}_1)}, \quad \beta_2 = -\beta_1, \quad \beta_2 = \tfrac{\tau\bar{\rho}_2\bar{S}_4}{-h(\bar{\rho}_2)} \\ \beta_4 &= -\beta_3, \quad \beta_5 = \tfrac{\tau\bar{\rho}_3\bar{S}_6}{-h(\bar{\rho}_3)}, \quad \beta_6 = -\beta_5. \end{aligned}$$

Example results displayed in the following are by this first-order scheme.

4.2 Numerical Examples

We first present the stop-and-go flow with (3.26), followed by a school zone example. In examples, we assume that $l_c = 1$ and $\tau = 1$. Note that different FDs are chosen in different examples.

Example IV.1.

Stop-and-go flow by System (3.26): we carried out the stop-and-go phenomenon by a microscopic model in section 2.2. In this example, we show that the 2x2 model (3.26) regenerates the unpredictable appearance of a traffic congestion comparable to stop-and-go flow. For this, we locally perturb uniform flow at three different places with the Gaussian pulse. A little later it amplifies the perturbations as in the ODE system, and then in the long run, solution remains periodic, capturing break-acceleration-break flow, see Figure 4.1. In this simulation,

$$V(\rho) = V_{\max}\big(1/(1 + e^{(\rho-0.25)/0.06}) - 3.72 \cdot 10^{-6}\big)$$

was used as in [27] by Kerner *et al.* . $s_{\min} = 1/3$, and $T = 10$ were used. We found that the number of initial perturbations corresponds to the number of break-acceleration flows, and the magnitude of the perturbation decides how fast the break-acceleration flow reaches. Larger perturbation, faster the flow stabilizes. Note that the initial condition needs to be chosen so that

$$v(x,0) - \frac{h(\rho(x,0))}{l_c} \le v(x,0) + \rho(x,0)V'(\rho(x,0)) \le v(x,0) \tag{4.1}$$

is satisfied. See [27, 25] for details. □

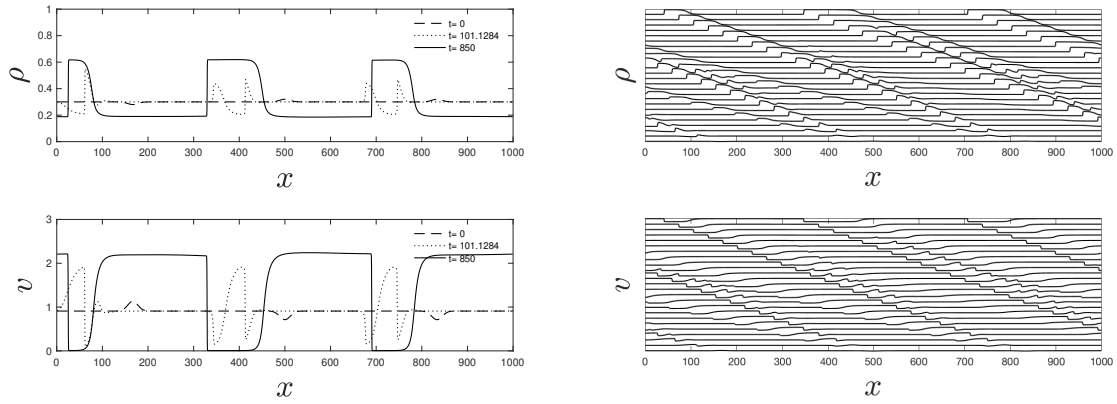

(a) Profiles of ρ and v at $t = 0,\ 100,\ 850$

(b) Time evolution of ρ and v

Figure 4.1: Instability of PDE system of (3.26)

Example IV.2.

School Zone Area by System (3.26): we simulate a school zone area that is the road that has a portion of variable speed limit, see the geometric structure in Figure 4.2a. We model this by spatially varying the speed limit in $V(\rho)$ in (3.26). In this simulation, Greenshields's model

$$V(\rho) = V_{\max}(1 - \rho)$$

was used and $V_{\max}$ is reduced by 1/3 in the school zone. $s_{\min} = 1$ and $T = 1/2$ were used. What cars experience is slowing down as entering the school zone, which creates car builds-ups going backwards, and then speeding up once they leave the school zone, see Figure 4.2b and 4.2c. The newly-developed $V(\rho)$ that has three phases was used and results are computed in Figure 4.3. This three phase $V(\rho)$ added more diffusive effect on the results.

This can be applicable to cases: the area where locally bad weather is affected, or the road that has a poor condition such as unpaved road so speed limit has to be reduced [40, 35]. □

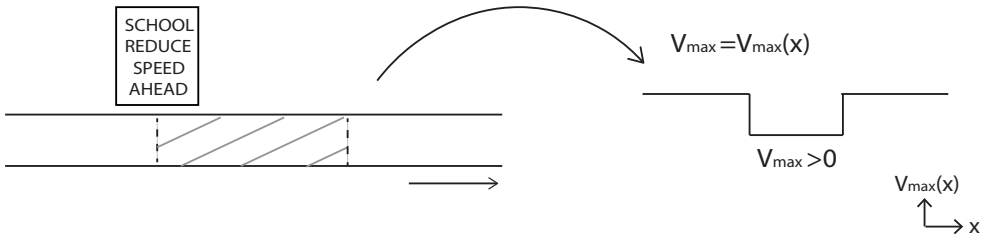

(a) Schematic for single-lane traffic flow through school zone

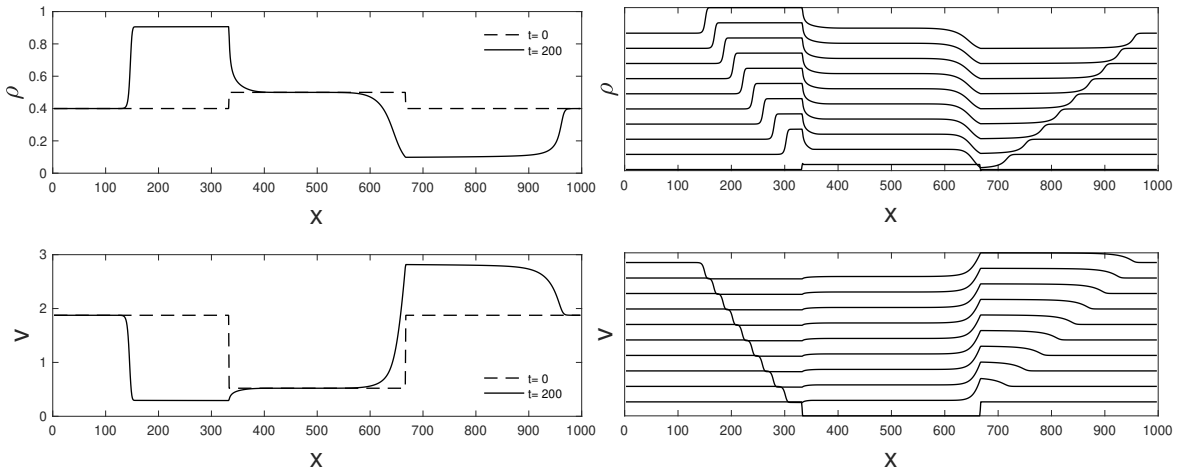

(b) Profiles of ρ and v at $t = 0,\ 200$

(c) Time evolution of ρ and v

Figure 4.2: Example IV.2 results by (3.26)

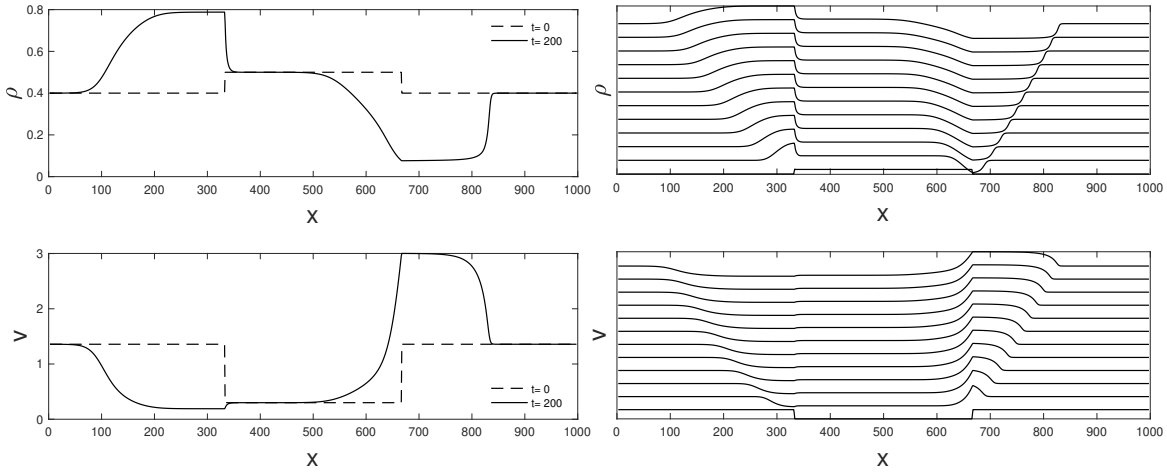

(a) Profiles of ρ and v at $t = 0,\ 200$

(b) Time evolution of ρ and v

Figure 4.3: Example IV.2 results by (3.26) with three-phase $V(\rho)$

We now present examples of both Type 1 and 2 models. We assume that $l_c = 1$ and $\tau_{lc} = 1$ for Type 1 and $\tau = 1$ for Type 2.

Example IV.3.

Lane Closure by (3.31): in this example, we consider the three-lane traffic flows where a lane drop is included. This circumstance may be attributed to a non-uniform geometry of roadways or an accident which necessitates a lane block and therefore lane switches. It is a trouble spot where there is chronic congestion or bottleneck, so it has been attracted attention to many researchers, see [41, 28, 42]. See Figure 4.4a for the road designed for this simulation. This lane-drop is then modeled by reducing the speed limit in lane 1 gradually to zero over the taper from three lanes to two. In this simulation,

$$V(\rho) = V_{\max}(1 - \rho),$$

and $V_{\max}$ in lane 2 and 3 are assigned to be 10% less than lane 1. Different speed limits are imposed as to the very left lane is reserved for faster-moving or passing vehicles under traffic laws. $s_{\min} = 2$, $R = 0.5$, and $\alpha = 0.01$. Putting initial density and speed uniformly in lane 2 and 3, and linearly decreasing density and speed to zero over the road taper in lane 1, reports the result in Figure 4.4b and its time evolution in Figure 4.4c. Because lane 1 ends, lane switch occurs to the right lanes, and this leads to traffic bottlenecks. We found that different initial data makes the results ended differently. Lighter initial density less than about $\rho = 0.3$ does not result in traffic bottleneck at all, as opposed to traffic bottleneck is observed over all lanes with denser initial density. Our results show that shock waves in ρ in all lanes propagates backwards with similar speed but little different strength. Larger $s_{\min}$, closer the shock strength in ρ_i for all i. This is because it leaves more minimal space

to allow cars to merge in, and this reduces the difference in shock strengths in each lanes. This also can be observed in (3.28) by rearranging,

$$s_{\min}\Big(\frac{1}{\rho_j} - 1\Big) > V(\rho_i).$$

As $s_{\min}$ gets larger, more chances of lane change condition to be satisfied and it affects the results in speed and strength of shock.

As a reference computation, we add a comparison with the scalar lane-aggregate model (3.18) by constructing $n(x)$ according to the road set up, see Figure 4.5a. It illustrates the accuracy and robustness of the model (3.31) especially the source terms, see Figure 4.5b. Propagation of shock speed and strength are not exactly same because the scalar lane-aggregate model (3.18) and Type 1 multilane model (3.31) in its summation form do not fully agree. □

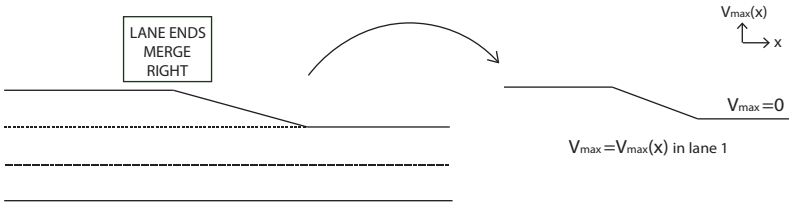

(a) Schematic for multilane traffic flow through lane closure

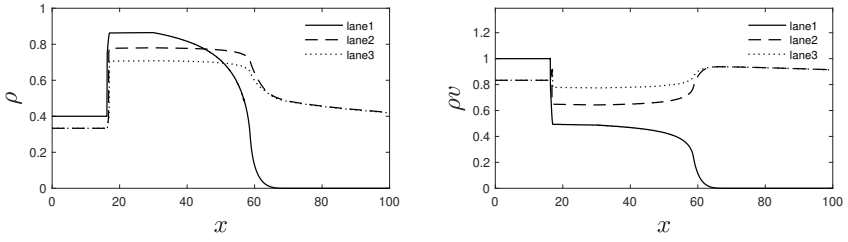

(b) Profiles of ρ and $\rho V(\rho)$ in each lane at $t = 70$

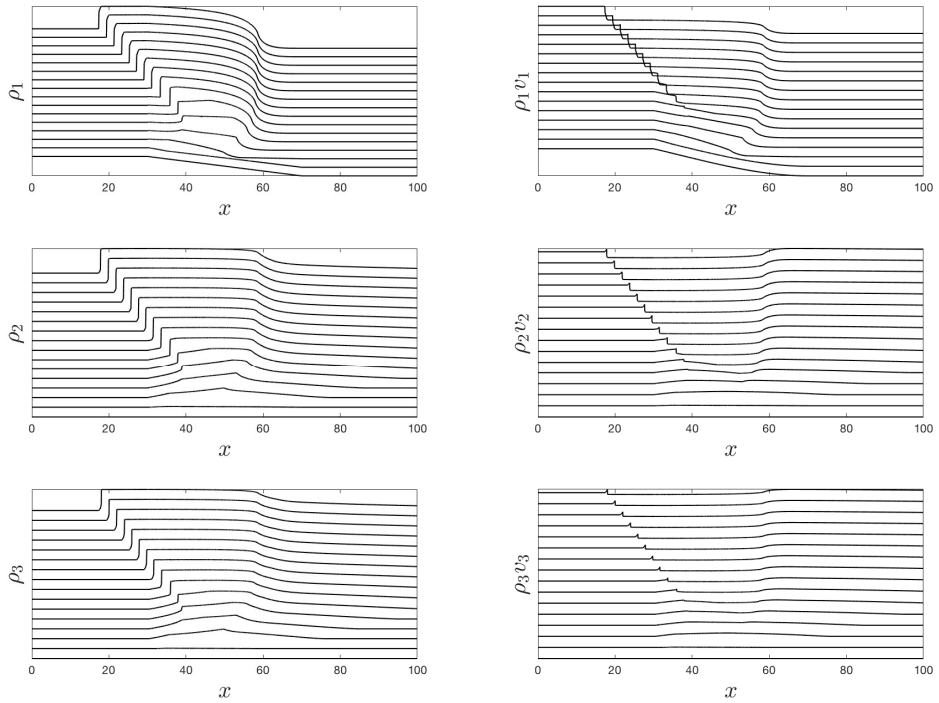

(c) Time evolution of ρ and ρv

Figure 4.4: Example IV.3 results by (3.31)

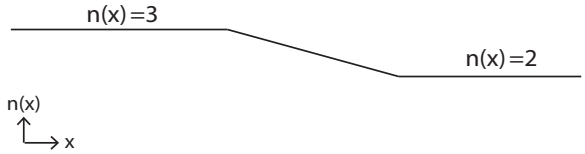

(a) $n(x)$ in (3.18) for the lane closure example

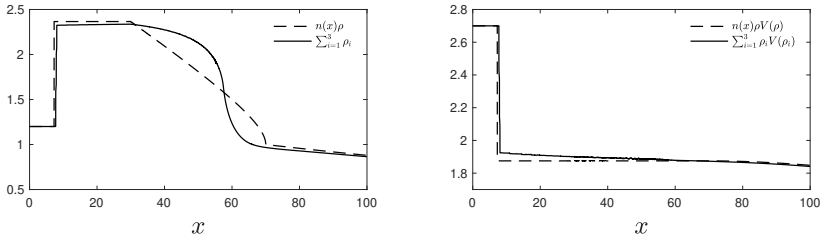

(b) Comparison of cumulative ρ and $\rho V(\rho)$ at $t = 70$ in lane drop simulation solved by (3.18), shown in dashed line, and by (3.31), shown in solid line. In this simulation speed limit in all lanes is assigned to be identical.

Figure 4.5: Example IV.3 results by (3.31) with (3.18)

Example IV.4.

Variable Speed Limit in Multilane by (3.33): in this example, we compute similar scenario of Example IV.2 but on a multilane road. Imagine a case where a road work is going on the shoulder of one side, which implicitly have drivers slow down to work-zone speed limit when workers are present. See Figure 4.6a for an example of three-lane roadways that has a construction area on a shoulder of lane 1. Traffic flow in this environment can be computed by changing speed limit in $V(\rho)$ in (3.33). In this computation, we present a comparison with and without lane changing effect. When the lane changing is not allowed, only intra-lane acceleration plays a role with no vehicle exchange and consequently no inter-lane acceleration is involved. See Figure 4.6b. In this simulation,

$$V(\rho) = V_{\max}(1 - \rho)$$

was used. $s_{\min} = 1$, $T = 1/3$, $\tau_{lc} = 2$, $\alpha = 0.1$, and $R = 0$. Although vehicles gradually move downstream in lane 1 causing rarefaction wave, vehicles are backed

up backwards forming relaxed shock-like wave due to the reduction in speed limit ahead. Meanwhile, with homogenous initial conditions, ρ and v keep uniform flow in the other lanes due to no interruption. See Figure 4.6c.

When the lane change is allowed, vehicles move away from lane 1 to lane 2 and lane 3, and eventually stabilizes. See Figure 4.7. We put results with and without the lane change effect together. The traffic queue in lane 1 when lane changing was not allowed is found to be alleviated because of lane changes, see Figure 4.8. We plot a trajectory of a vehicle in lane 1 calculated by v_1 computation, when lane changing is allowed. This is then compared by the trajectory when the lane changing is not allowed, see Figure 4.9. This provides it takes 29.60 unit time faster to get through the congestion when lane changing is allowed. $\square$

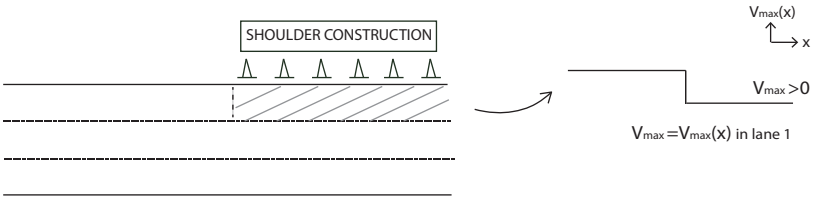

(a) Schematic for Example IV.4

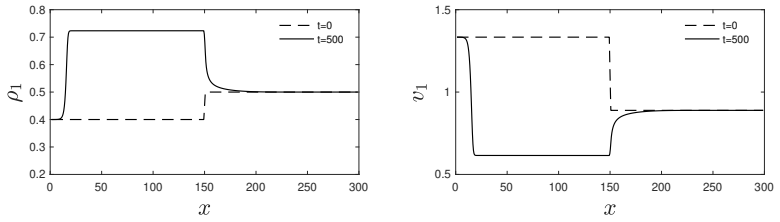

(b) Profiles of ρ and v at $t = 0,\ 500$ in lane 1

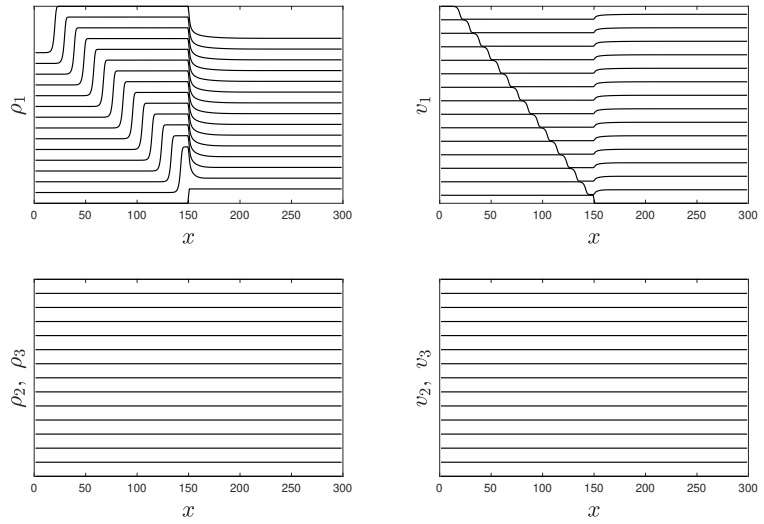

(c) Time evolution of ρ and v

Figure 4.6: Example IV.4 results by (3.33). In this simulation, $R = 0$.

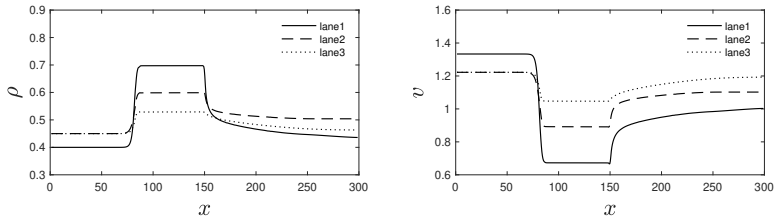

(a) Profiles of ρ and v at $t = 500$

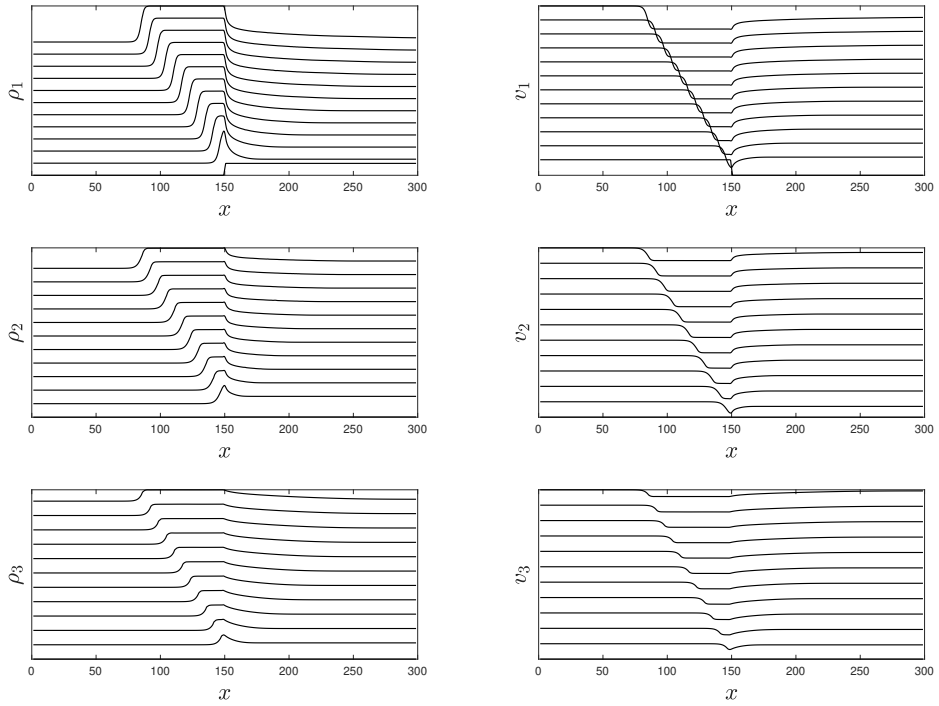

(b) Time evolution of ρ and v

Figure 4.7: Example IV.4 results by (3.33). In this simulation, $R = 0.3$.

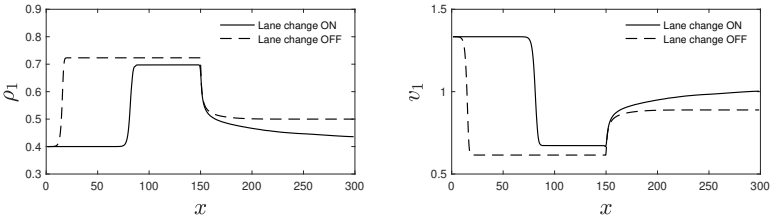

Figure 4.8: Example IV.4 results in lane 1 superimposed with and without effect of lane changes.

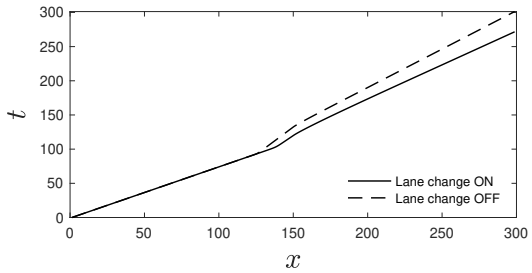

Figure 4.9: Trajectories of vehicles in lane 1 according to the computation of Example IV.4

Closing Remarks: Without traffic field data, it is hard to quantitatively conclude that results reflect the real traffic. However, it demonstrates that models developed in this dissertation are practicable to simulate interesting traffic examples. Moreover, all results show good qualitative agreement with daily life traffic experience.

CHAPTER V

Conclusion and Future Work

The field of traffic flow theory, computation, and its application is increasingly recognized as the era of autonomous vehicles approaches. Full understanding of mixed flow of human and autonomous vehicles requires good understanding of human-driving models, which are main theme of this dissertation. Furthermore, realistic and more accurate models make predictions better, and reduce the amount of money spent on gas, driving times and drivers' frustration levels because it improves the overall flow mobility. All above has been a motivation of this work.

We summarize the main contributions and new results of this dissertation, and discuss potential future applications. Data-driven fundamental relation of density and mean velocity was proposed, which is essential for macroscopic traffic flow models to be effective. We developed an acceleration equation that reflects microscopic characteristics, by making a link between microscopic and macroscopic variables, headway and density. The models were then generalized to multilane traffic models incorporating several features for lane changing: comparison of speeds and headways between lanes, mass exchanges, and inter-lane acceleration effects due to the car exchanges. We presented various numerical simulations, implemented by the Roe-type upwind scheme, including a lane reduction example from three to two lanes and

variable speed limits area in multilane.

This work opens up possibilities for other traffic challenges such as a network of roads, a road with signals, and roundabout problem. This work can be useful to control the flow. This is because prediction and estimation of throughput of the road can be used to enhance to maximize the flux without delaying vehicles on a road. This study may also deduce the lane-wise stop-and-go flow in multilane. In addition to this, multilane models can combine with multi-class to better understand the complex traffic phenomenon. Connected and autonomous vehicles will be on highways in a very near future. For this, modeling multilane with multi-class of platoons of connected and autonomous vehicles and human driving, which may require different lane-changing maneuver, is inevitable. Lastly, one ultimate goal may be to compare the multilane model to field data, which remains as future work.

APPENDIX

APPENDIX A

Data-driven three-phase FD

Using US 101 data, we optimize m and α in (3.6) by moving a window over the entire time and space. We obtain m and α by solving the optimization problem:

$$\min_{m,\alpha} \| \ln v - m \ln \rho - \ln \alpha \|_2^2$$

with a constraint $m \leq 0$. The result of the optimized m and α of US 101 data are shown in Figure A.1a and A.1c. Patterns in m and α do align with v. m and α are inversely related to ρ. Visual representation of the two parameters against ρ in Figure A.1b and A.1d supports the generalization form in (3.7).

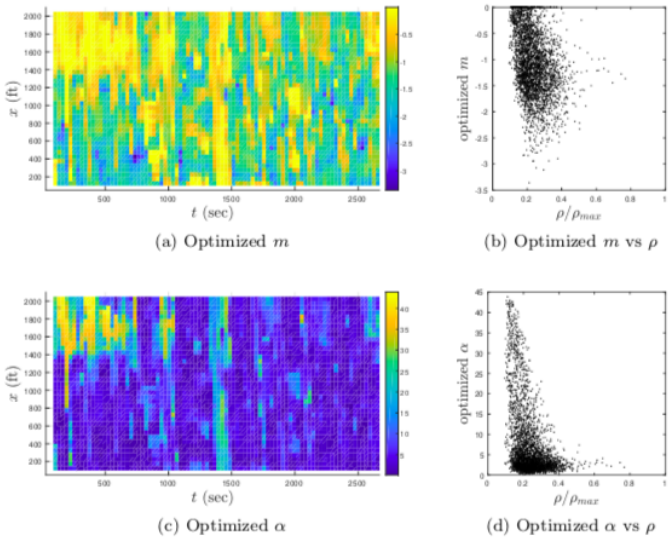

(a) Optimized m (b) Optimized m vs ρ

(c) Optimized α (d) Optimized α vs ρ

Figure A.1: Optimized m and α, and its relation with ρ

BIBLIOGRAPHY

BIBLIOGRAPHY

[1] A. Aw and M. Rascle. Resurrection of "Second Order" Models of Traffic Flow. *SIAM Journal on Applied Mathematics*, 60(3):916–938, January 2000.

[2] M. Bando, K. Hasebe, A. Nakayama, A. Shibata, and Y. Sugiyama. Dynamical model of traffic congestion and numerical simulation. *Physical Review E*, 51(2):1035–1042, February 1995.

[3] Masako Bando, Katsuya Hasebe, Ken Nakanishi, and Akihiro Nakayama. Analysis of optimal velocity model with explicit delay. *Physical Review E*, 58(5):5429, 1998.

[4] Masako Bando, Katsuya Hasebe, Ken Nakanishi, Akihiro Nakayama, Akihiro Shibata, and Yūki Sugiyama. Phenomenological Study of Dynamical Model of Traffic Flow. *Journal de Physique I*, 5(11):1389–1399, November 1995.

[5] Sylvie Benzoni-Gavage and Rinaldo M. Colombo. An n-populations model for traffic flow. *European Journal of Applied Mathematics*, 14(5):587–612, October 2003.

[6] Peter Berg, Anthony Mason, and Andrew Woods. Continuum approach to car-following models. *Physical Review E*, 61(2):1056–1066, February 2000.

[7] Sten Bexelius. An extended model for car-following. *Transportation Research*, 2(1):13–21, March 1968.

[8] Inc. Cambridge Systematics. NGSIM U.S. 101 Data Analysis. *https://data.transportation.gov/Automobiles/Next-Generation-Simulation-NGSIM-Vehicle-Trajector/8ect-6jqj*, December 2005.

[9] J. M. Del Castillo and F. G. Benítez. On the functional form of the speed-density relationship—I: General theory. *Transportation Research Part B: Methodological*, 29(5):373–389, October 1995.

[10] Robert E. Chandler, Robert Herman, and Elliott W. Montroll. Traffic Dynamics: Studies in Car Following. *Operations Research*, 6(2):165–184, April 1958.

[11] Kang-Ching Chu, Li Yang, R. Saigal, and K. Saitou. Validation of stochastic traffic flow model with microscopic traffic simulation. In *2011 IEEE Conference on Automation Science and Engineering (CASE)*, pages 672–677, August 2011.

[12] R. M. Colombo. A 2x2 hyperbolic traffic flow model. *Mathematical and Computer Modelling*, 35(5):683–688, March 2002.

[13] R. Courant, K. Friedrichs, and H. Lewy. On the Partial Difference Equations of Mathematical Physics. *IBM Journal of Research and Development*, 11(2):215–234, March 1967.

[14] Carlos F. Daganzo. Requiem for second-order fluid approximations of traffic flow. *Transportation Research Part B: Methodological*, 29(4):277–286, August 1995.

[15] J. L. Drake and Joseph L. Schofer. A Statistical Analysis of Speed-Density Hypotheses. *Highway Research Record 154*, pages 53–87, 1966.

[16] Denos C. Gazis, Robert Herman, and Renfrey B. Potts. Car-Following Theory of Steady-State Traffic Flow. *Operations Research*, 7(4):499–505, August 1959.

[17] Denos C. Gazis, Robert Herman, and Richard W. Rothery. Nonlinear Follow-the-Leader Models of Traffic Flow. *Operations Research*, 9(4):545–567, August 1961.

[18] S. K. Godunov. A difference method for numerical calculation of discontinuous solutions of the equations of hydrodynamics. page 37, 1959.

[19] Harold Greenberg. An Analysis of Traffic Flow. *Operations Research*, 7(1):79–85, February 1959.

[20] B.d. Greenshields, J.r. Bibbins, W.s. Channing, and H.h. Miller. A study of traffic capacity. *Highway Research Board proceedings*, 1935, 1935.

[21] Arvind Kumar Gupta and Sapna Sharma. Analysis of the wave properties of a new two-lane continuum model with the coupling effect. *Chinese Physics B*, 21(1):015201, 2012.

[22] Dirk Helbing and Andreas Greiner. Modeling and simulation of multilane traffic flow. *Physical Review E*, 55(5):5498–5508, May 1997.

[23] Edward N. Holland and Andrew W. Woods. A continuum model for the dispersion of traffic on two-lane roads. *Transportation Research Part B: Methodological*, 31(6):473–485, November 1997.

[24] Haijun Huang, Tieqiao Tang, and Ziyou Gao. Continuum modeling for two-lane traffic flow. *Acta Mechanica Sinica*, 22(2):131–137, April 2006.

[25] Rui Jiang, Qing-Song Wu, and Zuo-Jin Zhu. A new continuum model for traffic flow and numerical tests. *Transportation Research Part B: Methodological*, 36(5):405–419, June 2002.

[26] Rui Jiang, Qingsong Wu, and Zuojin Zhu. Full velocity difference model for a car-following theory. *Physical Review E*, 64(1):017101, June 2001.

[27] Boris S. Kerner and Peter Konhäuser. Cluster effect in initially homogeneous traffic flow. *Physical Review E*, 48(4):R2335, 1993.

[28] A. Klar and R. Wegener. A Hierarchy of Models for Multilane Vehicular Traffic I: Modeling. *SIAM Journal on Applied Mathematics*, 59(3):983–1001, January 1998.

[29] Axel Klar and Raimund Wegener. A hierarchy of models for multilane vehicular traffic II: Numerical investigations. *SIAM Journal on Applied Mathematics*, 59(3):1002–1011, 1998.

[30] Jorge A. Laval and Carlos F. Daganzo. Lane-changing in traffic streams. *Transportation Research Part B: Methodological*, 40(3):251–264, March 2006.

[31] Peter Lax and Burton Wendroff. Systems of conservation laws. *Communications on Pure and Applied Mathematics*, 13(2):217–237, May 1960.

[32] Peter D. Lax. *Hyperbolic Systems of Conservation Laws and the Mathematical Theory of Shock Waves*. SIAM, January 1973.

[33] Chin Jian Leo and Robert L. Pretty. Numerical simulation of macroscopic continuum traffic models. *Transportation Research Part B: Methodological*, 26(3):207–220, June 1992.

[34] Randall J LeVeque. Some Traffic Flow Models Illustrating Interesting Hyperbolic Behavior. page 11, 2001.

[35] Randall J. LeVeque. *Finite Volume Methods for Hyperbolic Problems*. Cambridge University Press, August 2002. Google-Books-ID: O_ZjpMSZiwoC.

[36] Jia Li, Qian-Yong Chen, Haizhong Wang, and Daiheng Ni. Analysis of LWR model with fundamental diagram subject to uncertainties. *Transportmetrica*, 8(6):387–405, November 2012.

[37] M. J. Lighthill and G. B. Whitham. On Kinematic Waves. II. A Theory of Traffic Flow on Long Crowded Roads. *Proceedings of the Royal Society of London. Series A, Mathematical and Physical Sciences*, 229(1178):317–345, 1955.

[38] Xiao-Yun Lu, P Varaiya, and Roberto Horowitz. Fundamental Diagram modeling and analysis based NGSIM data. In *12th IFAC Symposium on Control in Transportation System*, pages 367–374, 2009.

[39] Panos G. Michalopoulos, Dimitrios E. Beskos, and Yasuji Yamauchi. Multilane traffic flow dynamics: Some macroscopic considerations. *Transportation Research Part B: Methodological*, 18(4):377–395, August 1984.

[40] S. Mochon. An analysis of the traffic on highways with changing surface conditions. *Mathematical Modelling*, 9(1):1–11, January 1987.

[41] P. K. Munjal, Yuan-Shih Hsu, and R. L. Lawrence. Analysis and validation of lane-drop effects on multi-lane freeways. *Transportation Research*, 5(4):257–266, December 1971.

[42] K. Nassab, M. Schreckenberg, A. Boulmakoul, and S. Ouaskit. Effect of the lane reduction in the cellular automata models applied to the two-lane traffic. *Physica A: Statistical Mechanics and its Applications*, 369(2):841–852, September 2006.

[43] Gábor Orosz, R. Eddie Wilson, and Bernd Krauskopf. Global bifurcation investigation of an optimal velocity traffic model with driver reaction time. *Physical Review E*, 70(2), August 2004.

[44] Gábor Orosz, R. Eddie Wilson, Róbert Szalai, and Gábor Stépán. Exciting traffic jams: Nonlinear phenomena behind traffic jam formation on highways. *Physical Review E*, 80(4), October 2009.

[45] H. OZAKI. Reaction and Anticipation in the Car-Following Behavior. *Proc.of 12th International Symposium on Theory of Traffic Flow and Transportation*, pages 349–366, 1993.

[46] Harold J. Payne. MODELS OF FREEWAY TRAFFIC AND CONTROL. *MATHEMATICAL MODELS OF PUBLIC SYSTEMS*, 1971.

[47] Paul I. Richards. Shock Waves on the Highway. *Operations Research*, 4(1):42–51, February 1956.

[48] P. L Roe. Approximate Riemann solvers, parameter vectors, and difference schemes. *Journal of Computational Physics*, 43(2):357–372, October 1981.

[49] P. L Roe. Fluctuation and signals - a framework for numerical evolution problems. *Numerical Methods for Fluid Dynamics*, (Academic Press):219–257, 1982.

[50] P. L. Roe. Upwind differencing schemes for hyperbolic conservation laws with source terms. In Claude Carasso, Denis Serre, and Pierre-Arnaud Raviart, editors, *Nonlinear Hyperbolic Problems*, Lecture Notes in Mathematics, pages 41–51. Springer Berlin Heidelberg, 1987.

[51] Joel Smoller. *Shock Waves and Reaction—Diffusion Equations*. Springer Science & Business Media, December 2012. Google-Books-ID: lOIlBQAAQBAJ.

[52] Yuki Sugiyama, Minoru Fukui, Macoto Kikuchi, Katsuya Hasebe, Akihiro Nakayama, Katsuhiro Nishinari, Shin-ichi Tadaki, and Satoshi Yukawa. Traffic jams without bottlenecks—experimental evidence for the physical mechanism of the formation of a jam. *New Journal of Physics*, 10(3):033001, 2008.

[53] Eleuterio F. Toro. *Riemann Solvers and Numerical Methods for Fluid Dynamics: A Practical Introduction*. Springer Science & Business Media, April 2013. Google-Books-ID: zkLtCAAAQBAJ.

[54] R.T. Underwood. Speed, volume, and density relationships: Quality and theory of traffic flow. *Yale Bureau of Highway Traffic, New Haven, CT*, pages 141–188, 1961.

[55] G. B. Whitham. *Linear and nonlinear waves*. John Wiley & Sons, 1974.

[56] G. C. K Wong and S. C Wong. A multi-class traffic flow model – an extension of LWR model with heterogeneous drivers. *Transportation Research Part A: Policy and Practice*, 36(9):827–841, November 2002.

[57] Li Yang, Romesh Saigal, Chih-Peng Chu, and Yat-Wah Wan. Stochastic model for traffic flow prediction and its validation. In *Transportation Research Board 90th Annual Meeting*, 2011.

[58] H. Zhang and W. Jin. Kinematic Wave Traffic Flow Model for Mixed Traffic. *Transportation Research Record: Journal of the Transportation Research Board*, 1802:197–204, January 2002.

[59] H. M. Zhang. A non-equilibrium traffic model devoid of gas-like behavior. *Transportation Research Part B: Methodological*, 36(3):275–290, March 2002.